Earth's Future

RESEARCH ARTICLE
10.1029/2021EF002524

Special Section:
CMIP6: Trends, Interactions, Evaluation, and Impacts

Assessment of 21st Century Changing Sea Surface Temperature, Rainfall, and Sea Surface Height Patterns in the Tropical Pacific Islands Using CMIP6 Greenhouse Warming Projections

Laxmikant Dhage[1] and Matthew J. Widlansky[1]

[1]School of Ocean and Earth Science and Technology, Cooperative Institute for Marine and Atmospheric Research, University of Hawai`i at Mānoa, Honolulu, HI, USA

Key Points:

- CMIP6 projects increasing 21st-century rainfall for the equatorial Pacific, and in a broad part of the tropical north-western Pacific
- Rainfall changes are more uncertain for regions around many tropical Pacific Islands, such as Hawaii and American Samoa
- Assessing seasonal and interannual variability changes for particular warming amounts constrains uncertainty related to the global warming rate

Supporting Information:

Supporting Information may be found in the online version of this article.

Correspondence to:

M. J. Widlansky,
mwidlans@hawaii.edu

Citation:

Dhage, L., & Widlansky, M. J. (2022). Assessment of 21st century changing sea surface temperature, rainfall, and sea surface height patterns in the tropical Pacific Islands using CMIP6 greenhouse warming projections. *Earth's Future*, *10*, e2021EF002524. https://doi.org/10.1029/2021EF002524

Received 2 NOV 2021
Accepted 28 MAR 2022

Abstract Tropical Pacific Islands face unknown rates of future warming due to increased greenhouse gas emissions, but almost certain changing climate stresses. Continued global warming is projected to cause further changes to the mean conditions and variability of sea surface temperature (SST), rainfall, and sea surface height (SSH). Previous climate model simulations showed that the equatorial Pacific is likely to have greater increased rainfall, compared to elsewhere in the tropics. There is less certainty about future rainfall changes away from the equator, including around many of the numerous tropical Pacific Islands. Here, we assess the Coupled Model Intercomparison Project-phase 6 (CMIP6) as it relates to future changes of SST, rainfall, and SSH in the tropical Pacific. Focus is on the island regions of Hawaii, Guam, and American Samoa, as well as the Niño 3.4 region. We consider two development narratives of the 21st century by assessing the SSP2-4.5 and SSP5-8.5 experiments, and describe climate changes in the tropical Pacific relative to the recent historical conditions that are likely for either 1.5°C or 3°C of global mean surface temperature (GMST) warming above preindustrial levels. Consistent with prior-generation climate models, we find that future rainfall increases the most where SST warming is greatest, and also an overall increase of interannual variability associated with the El Niño-Southern Oscillation (ENSO) affecting rainfall and SSH. We describe changes in SST, rainfall, and SSH for particular warming amounts, and make comparisons with time-based climate assessments during the 21st century, which are relevant results toward better understanding uncertainty and supporting adaptation efforts in the tropical Pacific Islands.

Plain Language Summary We assess 21st century projected climate changes in the tropical Pacific using the latest generation of climate models that simulate Earth's response to increasing greenhouse gas emissions. Focus is on describing likely changes of rainfall, as well as sea surface temperature and height, for broad regions around Hawaii, Guam, American Samoa, and the other US-affiliated Pacific Islands. Although it remains unknown how much global warming will occur, the climate models are unequivocal that the tropical Pacific Ocean will continue to warm this century. We constrain this uncertainty by quantifying climate changes for particular warming amounts, such as 1.5°C or 3°C of global warming relative to preindustrial conditions. The surface of both the Earth and the tropical Pacific, specifically, have already warmed by more than 0.5°C. However, it is unknown when the 1.5°C or 3°C global warming amounts will occur. Some uncertainty also remains about regional climate changes associated with the future warming, such as for rainfall around Hawaii and American Samoa, whereas there is more consensus among models about the future rainfall increasing near the equator as well as near Guam in the north-western Pacific. Increasing equatorial rainfall is a consequence of that region projected to warm fastest and also suggests likely increasing climate variability affecting most tropical Pacific Islands.

1. Introduction

Future projections from the state-of-the-art Coupled Model Intercomparison Project-phase (CMIP6; Eyring et al., 2016) present an opportunity to reassess how the tropical Pacific climate is likely to change during the 21st century. Prior and current generations of climate models are unequivocal in projecting that the Earth's atmosphere and oceans will continue to warm with increasing greenhouse gas concentrations (Bindoff et al., 2013; Lee et al., 2021). Climate models also indicated that the future warming characteristics will almost certainly alter regional rainfall patterns (Doblas-Reyes et al., 2021), although there are large uncertainties about the rainfall

changes in the tropical Pacific (Power et al., 2021). Additionally, sea level rise is projected to occur nearly everywhere but at varying rates across the globe (Fox-Kemper et al., 2021).

The tropical Pacific contains a vast number of small islands, many of which have dense human populations and/or unique biological resources. Partly due to the isolated geography of the tropical Pacific Islands, along with most islands being either low-lying or having steep coastal topographies, their human communities and ecologies are especially vulnerable to climate changes (Keener et al., 2018). To support planning activities for successful adaptation to a future climate (e.g., Mcleod et al., 2019), this study will use the latest multi-model ensemble simulations from CMIP6 to assess the projected mean and variability changes of sea surface temperature (SST), rainfall, and sea surface height (SSH; variability only) in the entire tropical Pacific basin (i.e., bounded by 30°N/S). Focus will be on the US-affiliated Pacific Islands (USAPI) and in particular the island regions of Hawaii, Guam, and American Samoa. These islands, in addition to being separated by great distances between the north-central, north-western, and south-central parts of the Pacific Ocean, also have unique and varied climate characteristics (Annamalai et al., 2014).

Climate change is impacting the social-ecological-environmental system in the Pacific (Bograd et al., 2019). Oceanic warming is already stressing coral reefs around the tropical Pacific (e.g., Dutra et al., 2021), with associated consequences to fisheries (e.g., Venegas et al., 2019), tourism (e.g., Curnock et al., 2019), and potentially the buffering ability of reefs against coastal inundations from waves (e.g., Hoeke et al., 2013). The warming atmosphere is increasing evapotranspiration over the Pacific Islands (e.g., in Hawaii; Giambelluca et al., 2009), which will enhance the drought risk, especially for places that experience decreased rainfall (e.g., in Fiji; Deo, 2011). Furthermore, global sea levels are rising, and parts of the tropical Pacific are projected to experience much faster sea level rise than the global mean (Fasullo & Nerem, 2018). Ongoing land subsidence is further accelerating coastal sea level rise in certain areas (e.g., in the Samoan Islands; Han et al., 2019). Successfully adapting to climate changes affecting SST, rainfall, and SSH requires further understanding of their causes, as well as enhancing confidence in the future projections.

Assessment of prior climate projections (e.g., using CMIP5; Taylor et al., 2012) revealed a tendency for already wet places to get wetter in the future (Chou et al., 2013; Held & Soden, 2006). Since a warmer atmosphere can hold more moisture (i.e., a potentially higher specific humidity; Seager et al., 2010), many tropical Pacific Islands are likely to get wetter in the future (Annamalai et al., 2013). The wetter projection was especially robust in places with the fastest warming, such as in most of the equatorial Pacific (Huang et al., 2013). Future drying was projected in some other tropical regions, such as where the rate of warming is likely to be slower than the tropical average (e.g., in the south-eastern Pacific; Johnson & Xie, 2010). Overall, the CMIP5 projections showed clear patterns in the tropical Pacific of increasing atmospheric convergence and rainfall over the places projected to warm the fastest, and the opposite (i.e., divergence and drying) where the warming rate is slowest (Widlansky et al., 2013). In between these contrasting places of wet or dry future projections are vast regions of the tropical Pacific where the climate models either project small changes or are uncertain about the seasonal rainfall changes (Chadwick et al., 2013; Power et al., 2012). Uneven warming rates of the oceanic heat content will likewise also affect the regional amounts of thermal expansion in the Pacific Ocean, and hence the local rate of sea level rise (Fasullo & Nerem, 2018; Hay et al., 2015). Considering the strong coupling of these oceanic and atmospheric climate relationships, we will assess together the CMIP6 future change projections in SST, rainfall, and SSH. For the latter variable, we will only focus on assessing changes in variability, rather than long-term trends, because CMIP6 models do not independently resolve sea level rise associated with melting land ice, nor is the effect of vertical land motion included in the simulations.

In addition to causing changes in the climate mean state, greenhouse warming is expected to alter variability on seasonal-to-interannual timescales (Cai et al., 2021; Power et al., 2021). It has been suggested that the annual cycle of the tropical Pacific climate is likely to amplify with greenhouse warming (e.g., Timmermann et al., 2004), which would alter the seasonal differences in SST (Alexander et al., 2018; Dwyer et al., 2012), rainfall (Seth et al., 2013), and SSH (Widlansky et al., 2015). Any changes in the climatological annual cycle potentially could cause vast disruptions to society and biological processes. The El Niño-Southern Oscillation (ENSO) also interacts with the tropical Pacific annual cycle (Jin et al., 1994; Tziperman et al., 1994). Since ENSO is the dominant source of interannual variability in the tropical Pacific climate (McPhaden et al., 2020), changes in it could likewise have profound impacts to the marine and terrestrial environment as well as society (Holbrook et al., 2020; Lehodey et al., 2020).

Table 1
CMIP6 Models and Variables

Model name	Ocean resolution	Atmosphere resolution	"tos" and "ts"	"pr"	"zos"
ACCESS-CM2	100 km	250 km	Yes	Yes	Yes
ACCESS-ESM1-5	100 km	250 km	Yes	Yes	Yes
BCC-CSM2-MR	50 km	100 km	Yes	Yes	Yes
CAMS-CSM1-0	100 km	100 km	Yes	Yes	Yes
CESM2-WACCM	100 km	100 km	Yes	Yes	Yes
CIESM	50 km	100 km	Yes	Yes	Yes
CMCC-CM2-SR5	100 km	100 km	Yes	Yes	Yes
CMCC-ESM2	100 km	100 km	Yes	Yes	Yes
CanESM5	100 km	500 km	Yes	Yes	Yes
EC-Earth3	100 km	100 km	Yes	Yes	Yes
EC-Earth3-CC	100 km	100 km	Yes	Yes	Yes
EC-Earth3-Veg	100 km	100 km	Yes	Yes	Yes
FGOALS-f3-L	100 km	100 km	Yes	No	No
FGOALS-g3	100 km	250 km	Yes	Yes	Yes
FIO-ESM-2-0	100 km	100 km	Yes	Yes	Yes
GFDL-CM4	25 km	100 km	Yes	No	SSP5-8.5 only
GFDL-ESM4	50 km	100 km	Yes	Yes	Yes
IITM-ESM	100 km	250 km	Yes	No	No
INM-CM4-8	100 km	100 km	Yes	Yes	Yes
INM-CM5-0	50 km	100 km	Yes	Yes	Yes
IPSL-CM6A-LR	100 km	250 km	Yes	Yes	Yes
KIOST-ESM	100 km	250 km	Yes	No	Yes
MIROC6	100 km	250 km	Yes	Yes	Yes
MPI-ESM1-2-HR	50 km	100 km	Yes	Yes	Yes
MPI-ESM1-2-LR	250 km	250 km	Yes	Yes	Yes
MRI-ESM2-0	100 km	100 km	Yes	Yes	Yes
NESM3	100 km	250 km	Yes	Yes	Yes
NorESM2-LM	100 km	250 km	Yes	Yes	Yes
NorESM2-MM	100 km	100 km	Yes	Yes	Yes

Note. For each model, their respective ocean and atmosphere nominal resolutions are listed, along with notation of whether or not data is available for each of the variables that we analyzed. The following CMIP6 variable names (and their abbreviations) respectively describe SST, rainfall, and SSH: sea_surface_temperature (tos; 29 models), precipitation_flux (pr; 25 models), and sea_surface_height_above_geoid (zos; 26 models). We also used the surface_temperature (ts; 29 models) variable to calculate GMST warming amounts.

Many studies assessed how ENSO is projected to change in response to future greenhouse warming, using previous-generation and current-generation climate models (Berner et al., 2020; Cai et al., 2015; Collins et al., 2010; Fredriksen et al., 2020; Guilyardi et al., 2012; Stevenson, 2012; Taschetto et al., 2014; Wengel et al., 2021; Yeh et al., 2012). The majority of climate models are in consensus that the SST variability associated with ENSO is likely to increase, especially in the equatorial central Pacific (Cai et al., 2021, 2022). For rainfall specifically, the projected increase in interannual variability is even more robust across models compared to the SST changes (Ying et al., 2022; Yun et al., 2021), which has been interpreted using CMIP5 models to be associated with the effect of future increasing moisture being only partially mitigated by weakening atmospheric circulation (He & Li, 2019; Pendergrass et al., 2017). Here, we will briefly reassess the future projections of annual cycle and interannual variability changes using all of the currently available CMIP6 models (Table 1). Our focus will be on assessing climate changes that have so far remained either uncertain (e.g., seasonal rainfall patterns away from the equator) or relatively unstudied (e.g., SSH variability).

The major rainfall bands of the tropical Pacific tend to orient along where the trade winds converge, which is typically on the warm side of large-scale SST gradients, and are hence referred to as the Intertropical Convergence Zone (ITCZ; e.g., Broccoli et al., 2006) and South Pacific Convergence Zone (SPCZ; e.g., Widlansky et al., 2011). SSH variability, which is forced mostly by fluctuations in heat and momentum air-sea fluxes, tends to be largest near the ITCZ and SPCZ as well (Timmermann et al., 2010; Widlansky et al., 2014). Hence, successful simulation of the climate requires coupling of oceanic and atmospheric models.

Coupled climate models (e.g., CMIP5 and CMIP6) mostly resolve the observed features in SST, rainfall, and SSH, although the simulations always differ from observations to some extent. The amount that a simulation deviates from observations is called the model bias (i.e., the modeled minus observed condition during a historical epoch of overlapping data), which may be due to either location or amplitude errors, and occur in the mean state or variability. To mitigate the influence of biases, we utilize the common method of measuring future changes with respect to the historical (model) conditions, independent of the observations. Yet, model biases may directly influence the future projection. For instance, if compared to observations, the simulated ITCZ or SPCZ is either too strong or weak, or out of position, then the historical bias may hinder confidence in the future change (e.g., of rainfall). We will briefly summarize the historical performance of CMIP6 but leave for further study a detailed assessment of relationships between model biases and projected changes.

Most of the uncertainty about how much the climate will change during the 21st century is because the future amounts of greenhouse gas emissions are unknown. There is also a large spread (or sensitivity) across models in their warming response to increased radiative forcing (Dong et al., 2020; Meehl et al., 2020). The range in rates and total amounts of warming contributes to unknowns about all potential climate changes (e.g., affecting not only the future SST, but also rainfall and SSH). To develop a protocol for simulating a range of potential future climate scenarios, in preparation for the IPCC sixth Assessment Report (AR6), a set of shared socioeconomic psathways (SSPs; O'Neill et al., 2014; Riahi et al., 2017) were developed and partnered to representative concentration pathways (RCPs). Combined, the

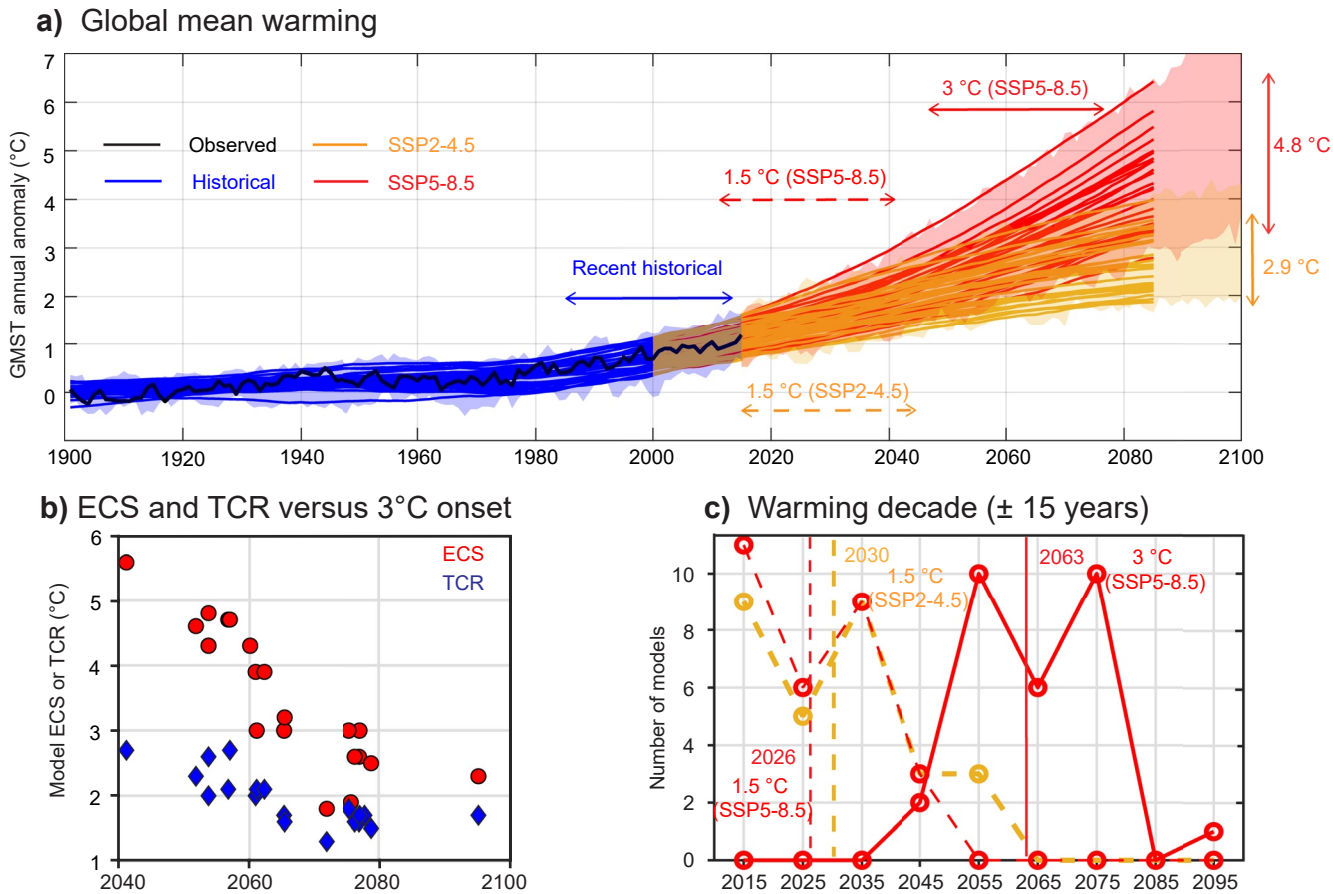

Figure 1. Observed and projected global mean warming. (a) GMST annual anomalies from 1900 to 2100 relative to 1850–1900 using the following data: observed (black), historical (blue), SSP2-4.5 (yellow), and SSP5-8.5 (red). For CMIP6 data, shading indicates the intermodel spread of the annual anomalies and lines indicate the 30-year running averages of individual models, which are used to determine for each model the future epochs of when warming amounts occur. Horizontal arrows indicate the average epochs for SSP2-4.5 (1.5°C only) and SSP5-8.5 (dashed and solid distinguish 1.5°C or 3°C of warming). The intermodel ranges during the last 30-year epoch (2071–2100) of both experiments are indicated by vertical arrows. (b) ECS and TCR values for available models from Meehl et al. (2020) versus the year when 3°C of warming occurs for the SSP5-8.5 experiment. (c) Number of models that reach warming amounts by the middle decade of the running 30-year epoch for the future projections (SSP2-4.5: yellow, 1.5°C; SSP5-8.5: dashed and solid red, 1.5°C and 3°C, respectively).

SSP-RCP partnerships describe the additional radiative forcings associated with a variety of global development possibilities (Rogelj et al., 2018).

We chose here to consider two distinct narratives of the 21st-century development; one is a fossil-fueled economy and the other is more middle-of-the-road as far as the additional amount of greenhouse gases emitted (i.e., simulated by the SSP5-8.5 and SSP2-4.5 experiments, respectively). From these experiments, we will assess the climate changes that are likely when the global mean surface temperature (GMST) warms by 1.5°C or 3°C relative to the 1850–1900 epoch of the historical experiment (Figure 1a and Table 2), which approximates the amount of warming since preindustrial climate conditions (Allen et al., 2018). Such a methodology of describing climate changes associated with particular warming levels, which is sometimes referred to as the "time-shift method" (Herger et al., 2015), is increasingly being utilized (e.g., by the IPCC AR6; Lee et al., 2021). We note that by describing climate changes as a function of warming amount—instead of time—we attempt to reduce the uncertainty associated with the widely ranging temperature sensitivities of future simulations (Figure 1b). The spread in projections of GMST is mostly because models tend to warm at different rates during the 21st century

Table 2
Comparison of Warming Amounts Between Regions, Variables, and Reference Epochs

GMST relative to early historical (1850–1900)	GMST relative to recent historical (1985–2014)	Tropical Pacific SST relative to early historical (1850–1900)	Tropical Pacific SST relative to recent historical (1985–2014)
1.5°C	0.8°C	1.2°C	0.7°C
3.0°C	2.3°C	2.3°C	1.8°C

Note. Future changes in the GMST and tropical Pacific SST are relative to either the early or recent epochs of the CMIP6 historical experiment. Figure 1 shows the future epochs when 1.5 or 3°C of GMST warming are projected to occur, relative to the early historical epoch.

(i.e., the transient climate response; TCR) and are expected to reach different temperature equilibriums (referred to as equilibrium climate sensitivity; ECS) for the same amount of radiative forcing prescribed (Meehl et al., 2020). Furthermore, the CMIP6 models exhibit a higher climate sensitivity compared to previous-generation models (Zelinka et al., 2020), which suggests that studies assessing only the end-of-century projections from the SSP5-8.5 experiment may be greatly overestimating the likely amount of 21st-century climate changes.

The remainder of the paper is organized as follows. In the next section, we explain the observations and CMIP6 data that we make comparisons between for measuring model biases, along with the methodology that we use for assessing future climate changes. Section 3 presents the assessment results, which include description of the CMIP6 bias, future warming pattern and amount, seasonal changes to rainfall, and seasonal-to-interannual variability changes affecting SST, rainfall, and SSH. We summarize the CMIP6 climate change projections in Section 4, and then examine remaining unknowns about how the tropical Pacific climate will change during the 21st century. We also discuss the implications of these results for adaptation efforts in the tropical Pacific Islands.

2. Materials and Methods

2.1. Data

We assessed oceanic and atmospheric climate projections in the tropical Pacific (30°S–30°N, 100°E−70°W) using monthly output from 29 CMIP6 models (Table 1; Eyring et al., 2016). We chose the models to maximize the data available for assessment of SST, rainfall, and SSH with respect to the GMST (i.e., amount of global warming). The CMIP6 models vary somewhat in complexity, especially regarding spatial resolutions of their respective atmospheric and oceanic simulations. For each variable and model, we first interpolated the data onto common spatial grids using the Earth System Modeling Framework regridding software (https://earthsystemmodeling.org/regrid/). We linearly interpolated the SST, surface temperature, and SSH to a 1° latitude × 1° longitude grid, and used a 2.5° latitude × 2.5° longitude grid for conservatively regridding rainfall since the atmospheric model components typically have coarser resolutions than the ocean (Table 1). We considered one realization of the climate from each model (e.g., "r1i1p1f1," according to the CMIP6 naming protocol for simulation variants) during the historical (1850–2014) and future (2015–2100) epochs. In addition to the historical experiment, we considered two future experiments (SSP2-4.5 and SSP5-8.5).

To assess the CMIP6 ability to simulate the observed climate, we compared the multi-model mean to satellite measurements of SST, rainfall, and SSH during the overlapping historical epoch (nominally 1985–2014, except since 1993 for SSH because of the more limited satellite-based observations of sea level). We also compared the GMST from each model since 1900 with the global average of the Met Office Hadley Centre/Climatic Research Unit global surface temperature data set (HadCRUT5; Morice et al., 2021). The other observations, respectively, are from the following three data products: (a) NOAA Extended Reconstructed SST, version 5 (Reynolds et al., 2002); (b) Global Precipitation Climatology Project (GPCP), version 2.3 (Adler et al., 2018); and, (c) SSALTO/DUACS multimission data set distributed by the European Copernicus Marine Environment Monitoring Service (CMEMS), global ocean gridded SSH (Pujol et al., 2016). We used annual means of the GMST and monthly means of the other observations. The SST and rainfall observations are on the same spatial grids as the regridded CMIP6 data (1.0° and 2.5° latitude/longitude, respectively). We linearly interpolated the SSH observations from their 0.25° latitude/longitude grid to match the resolution of our regridded SSH CMIP6 data (1.0° latitude/longitude). Note that these regridding procedures were designed to minimize potentially aliasing the results, since we almost always either left unchanged or coarsened the original horizontal resolutions of both observations and CMIP6 (e.g., only 1 out of 29 models for rainfall has a nominal atmospheric resolution that is coarser than 250 km, or about 2.5° latitude/longitude; Table 1).

2.2. Methods

We used seasonal averages of May–October and November–April to characterize how the tropical Pacific climate changes, respectively, from the 6 months around boreal summer to the other months around boreal winter. (Or, equivalently, we characterized the austral winter and summer 6-month averages.) On a location-by-location basis, we also calculated the annual cycles for each of SST, rainfall, and SSH according to their ranges from the minimum month to the maximum (e.g., if the local monthly SST varies from 24°C to 26°C on average, then the annual cycle range is 2°C). Finally, we assessed interannual variability, which we defined as the standard deviation of

monthly anomalies that were calculated by first removing the annual cycles, next subtracting the long-term linear trends, and finally applying a 12-year high-pass filter (Thomson & Emery, 2014). Performing the two latter steps helped to isolate interannual variability from any changes on decadal or longer timescales (Power et al., 2021). Also, for SSH only, we removed the respective global mean SSH anomaly at each month to avoid effects of long-term sea level drift present in the models (Widlansky et al., 2015) or sea level rise in the case of the satellite altimetry observations (Fasullo & Nerem, 2018).

Before assessing future changes, we assessed the CMIP6 biases by calculating differences between the multi-model mean of the historical experiment and observations during overlapping epochs of the data. We performed the historical minus observed assessment on all variables (i.e., SST, rainfall, and SSH) and timescales (i.e., seasonal averages, annual cycles, and interannual variabilities). Results of the bias assessment are presented in Section 3.1.

We calculated the future projections for each model individually and also using the multi-model mean. The climate changes are with respect to the last 30 years of the historical experiment (1985–2014) for the respective models. Assuming that model biases are consistent between the historical and future experiments, the future minus historical comparison helps to distinguish between the climate change signal and any model errors. Future projections are presented spatially as raw changes, which preserves the variable units as either °C (SST), mm/day (rainfall), or cm (SSH). For the focus areas of Hawaii, Guam, American Samoa, and the Niño 3.4 region (outlined in Figure 2), we also show percentage changes (i.e., by dividing the future minus historical difference by the historical climatology; units of %).

Our climate change assessment seeks to reduce the uncertainties associated with both the amount of future radiative forcing and the warming sensitivities of CMIP6 models (Dong et al., 2020; Meehl et al., 2020; Zelinka et al., 2020). We attempt this reduction of climate change uncertainty by determining the future rainfall and SSH conditions that occur when the amount of global warming (i.e., GMST) reaches either 1.5°C or 3°C relative to the early historical epoch (i.e., 1850–1900), instead of basing our assessment on particular temporal changes. These warming amounts are equivalent to GMST changes of 0.8°C or 2.3°C, respectively, since the recent historical epoch (i.e., 1985–2014; Table 2). We also note that overall, the tropical Pacific is projected to warm slower than the GMST change (e.g., relative to the early historical epoch, the 3°C global warming amount is equivalent to 2.3°C in the tropical Pacific; or, 1.8°C relative to the recent historical epoch). Both the SSP2-4.5 and SSP5-8.5 experiments resolve climate changes when the GMST warms by 1.5°C, but only the latter experiment continues to warm to 3°C or more (Figure 1a). The majority of models project reaching these respective warming amounts as soon as the 2020s (1.5°C) or 2060s (3°C) for the SSP5-8.5 experiment (Figure 1c). For the SSP2-4.5 experiment, warming happens slower, and the timing is more uncertain across models (see also Section 3.2).

To combine the different future scenarios for a certain degree of warming (only the SSP5-8.5 experiment is considered for the 3°C change), we first smoothed the historical and future GMST time series using a 30-year running-window average for each model separately. We perform the 30-year averaging to minimize fluctuations associated with ENSO variability, since our objective is to determine when future mean warming amounts are projected to occur for each model, independent of any internal climate variability. Next, by assessing the smoothed SST time series (Figure 1a), we determined the future times when the models project warming by 1.5°C or 3°C with respect to their early historical 51-year averages (1850–1900). We added ±15 years to these times of 1.5°C or 3°C warming, thus defining 30-year epochs of the 21st century for each model (Figure 1c). Note that the 30-year epochs overlap between the historical and future experiments during the early 21st century (e.g., 2001–2030). Finally, we assessed the tropical Pacific climate changes for when GMST warming of 1.5°C or 3°C occurs. In the next section, after first describing the CMIP6 biases, we report the future climate changes with regard to the seasonal mean, annual cycle, and interannual variability.

3. Results

3.1. Historical Mean-State Biases

Similar to previous-generation coupled climate models (e.g., CMIP5), the CMIP6 models simulate a tropical Pacific climate resembling observations. CMIP6 models depict large-scale features of the observed ocean, such as the SST gradient between the West Pacific warm pool (enclosed by the 28°C isotherm) and an overall much cooler tropical eastern Pacific (Figure 2). Likewise, the major rainfall bands of the tropical Pacific are simulated

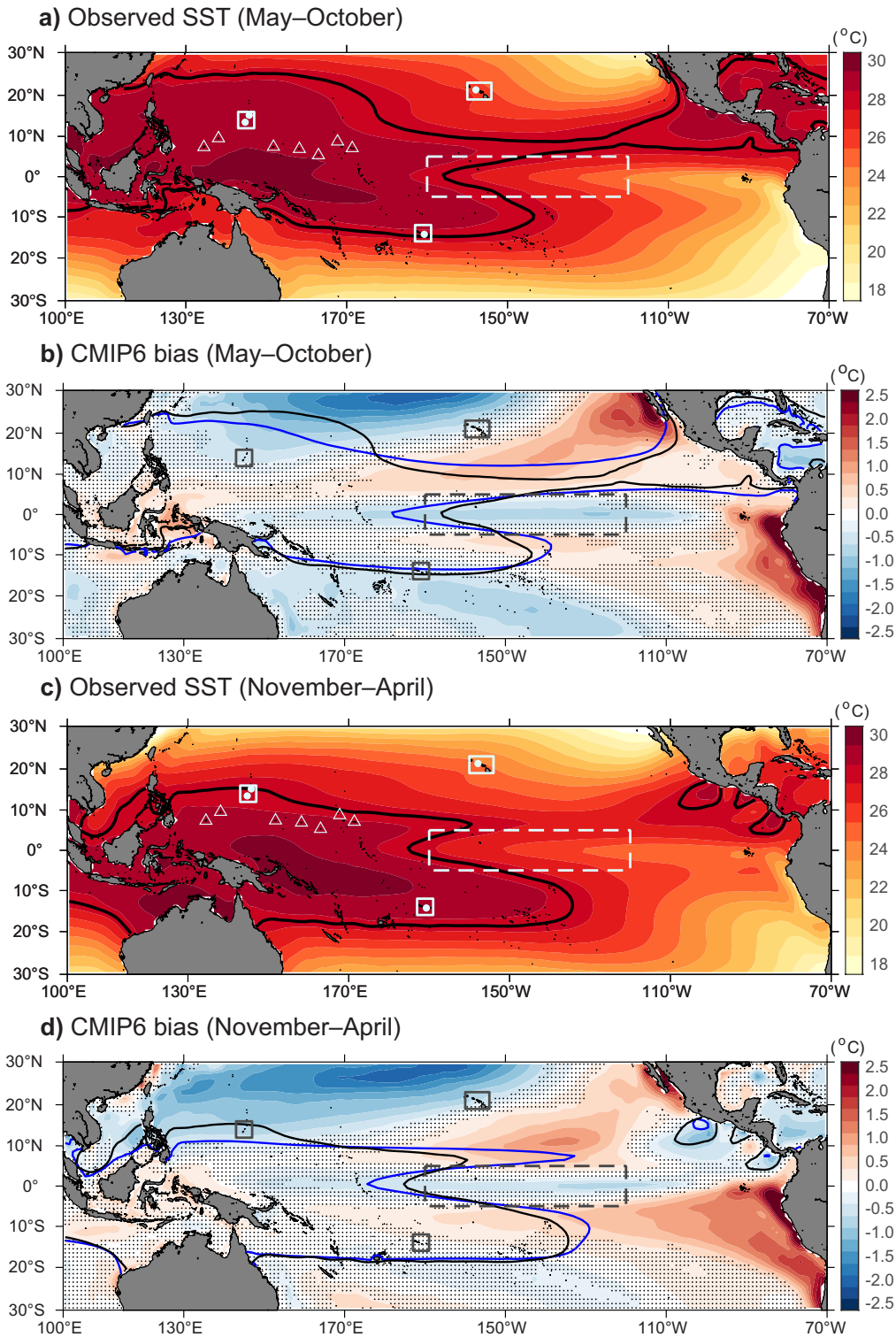

Figure 2. Observed SST and CMIP6 bias during 1985–2014 (°C, color bars). (a, c) Observed seasonal mean SST during May–October and November–April, respectively. (b, d) Multi-model mean SST bias for the historical experiment relative to observations during the respective seasons. Contour lines depict the 28°C isotherm for the observed (black) and historical (blue) conditions. Black stippling indicates that less than 66% of models agree on the sign of SST bias. Regions are indicated in all maps as follows: solid boxes denote the island regions from north-to-south of Hawaii, Guam and the Northern Mariana Islands, and American Samoa; and the dashed rectangle encloses the Niño 3.4 region. In Figures 2a and 2c, as well as Figures 4a and 4b, circles indicate the capitals of the US states and territories (Honolulu, Hagåtña, Saipan, and Pago Pago), and triangles denote other places in the USAPI.

in some way by CMIP6 (Figure 3; the 5 mm/day contour outlines heavy rainfall associated with the ITCZ and SPCZ in the NH and SH, respectively). Yet, persistent biases remain in both the simulated SST (Figures 2b and 2d) and rainfall (Figures 3b and 3d), which should be considered in the context of assessing future climate change projections. Here, we summarize the characteristics of mean-state biases (patterns and amounts) in the CMIP6 historical experiment depictions of SST and rainfall, as well as SSH (biases in the temporal variability will be noted in Section 3.4 when we consider future interannual changes).

The CMIP6 simulation of SST is mostly too warm in the eastern Pacific and too cool in the central and western Pacific (Figures 2b and 2d). Along the entire South American Coast, there is a substantial warm bias, which is largest near the equator (exceeding 2.5°C). In the equatorial central Pacific, the simulated SST is somewhat too cool (i.e., the so-called cool tongue bias of −1°C around the Niño 3.4 region). The coldest biases are in the subtropical north-central Pacific (exceeding −2.0°C poleward of 25°N from 170°E to 160°W; i.e., northwest of Hawaii), which along with considering the warm bias in the north-eastern Pacific (above 2°C near and offshore of the North American Coast), indicate that there are pronounced differences in the large-scale SST gradients compared to observations. Near Hawaii in CMIP6, the zonal gradient of SST is diminished and the meridional gradient is enhanced, whereas the zonal gradient between the warm pool and Niño 3.4 region is too large compared to observations. The seasonal differences in these SST biases are mostly small although the north-eastern Pacific is especially too warm during boreal summer (Figure 2b). Consistent with ocean thermodynamics, the SSH bias pattern (Figure S1 in Supporting Information S1) generally mirrors the SST biases (e.g., CMIP6 sea levels are too high where the simulated upper-ocean is too warm, such as in the tropical north-eastern Pacific). Both the SST and SSH biases are likely the outcome of errors that exist in the CMIP6 simulation of heat and momentum surface fluxes, and the resulting ocean circulation (J. L. Li et al., 2020).

Rainfall biases in CMIP6 are especially large within or near the margins of where heavy rainfall is observed (Figure 3) and indicate either deficiencies in the location or magnitude of simulating the major rainfall bands (i.e., the ITCZ and SPCZ). The CMIP6 historical climate is generally too dry along the equator, and too wet in the off-equatorial areas. The monsoonal wet season around Guam during boreal summer is much too wet, and that wet bias is more severe toward the east, extending broadly along 10°N into the central Pacific and affecting many of the USAPI (Figure 3b; see Figure 2 for all of the island locations). The off-equatorial South Pacific is also mostly too wet (i.e., in the SPCZ region including around American Samoa), especially during austral summer (Figure 3d). Rainfall biases in the SH are greatest near the eastern boundary of the SPCZ and extend toward South America, which is indicative of the so-called double-ITCZ bias commonly seen in climate models (e.g., Oueslati & Bellon, 2015). Also of note is the dry bias along the southern boundary of the SPCZ, which is larger during austral summer (i.e., near 25°S between 170°E and 150°W). Biases near Hawaii are smaller during both seasons. However, we note that none of the atmospheric models in CMIP6 have horizontal resolutions (Table 1) suitable for resolving rainfall characteristics around complex island topography. Likewise, the satellite rainfall observations do not fully describe the rainfall characteristics as recorded by rain gauges in Hawaii (Longman et al., 2021). Many parts of Hawaii are in fact much wetter than either measured by satellites or simulated in global climate models (Lauer et al., 2013), which is a bias that must be considered when assessing the projected changes.

The simulated rainfall and SST patterns in the tropical Pacific are mostly consistent in the sense that the biases share similar pattern characteristics (i.e., comparing the sign of CMIP6 biases in Figures 2 and 3). Regions warmer than observed tend to be too wet (e.g., in the tropical south-central and south-eastern Pacific) and cooler locations have a dry bias (e.g., around and west of the Niño 3.4 region). Many of the tropical Pacific Islands are located near where some of the largest rainfall biases occur (e.g., Guam and American Samoa, especially during their respective wet seasons; Figures 3b and 3d). Hawaii is further away (north) of the positive rainfall bias in the central Pacific, which is associated with the simulated ITCZ being too broad and wet. Considering the apparent linkages between the SST and rainfall patterns, we will assess the projected climate changes in the context of knowing that pronounced biases exist in the CMIP6 simulation of these variables, which in some places are much larger in magnitude compared to the future changes.

3.2. Future Warming

There is no uncertainty in CMIP6 that the tropical Pacific will warm during the 21st century (Figure 4), although there is large spread across experiments and models about how much global warming will occur by 2100

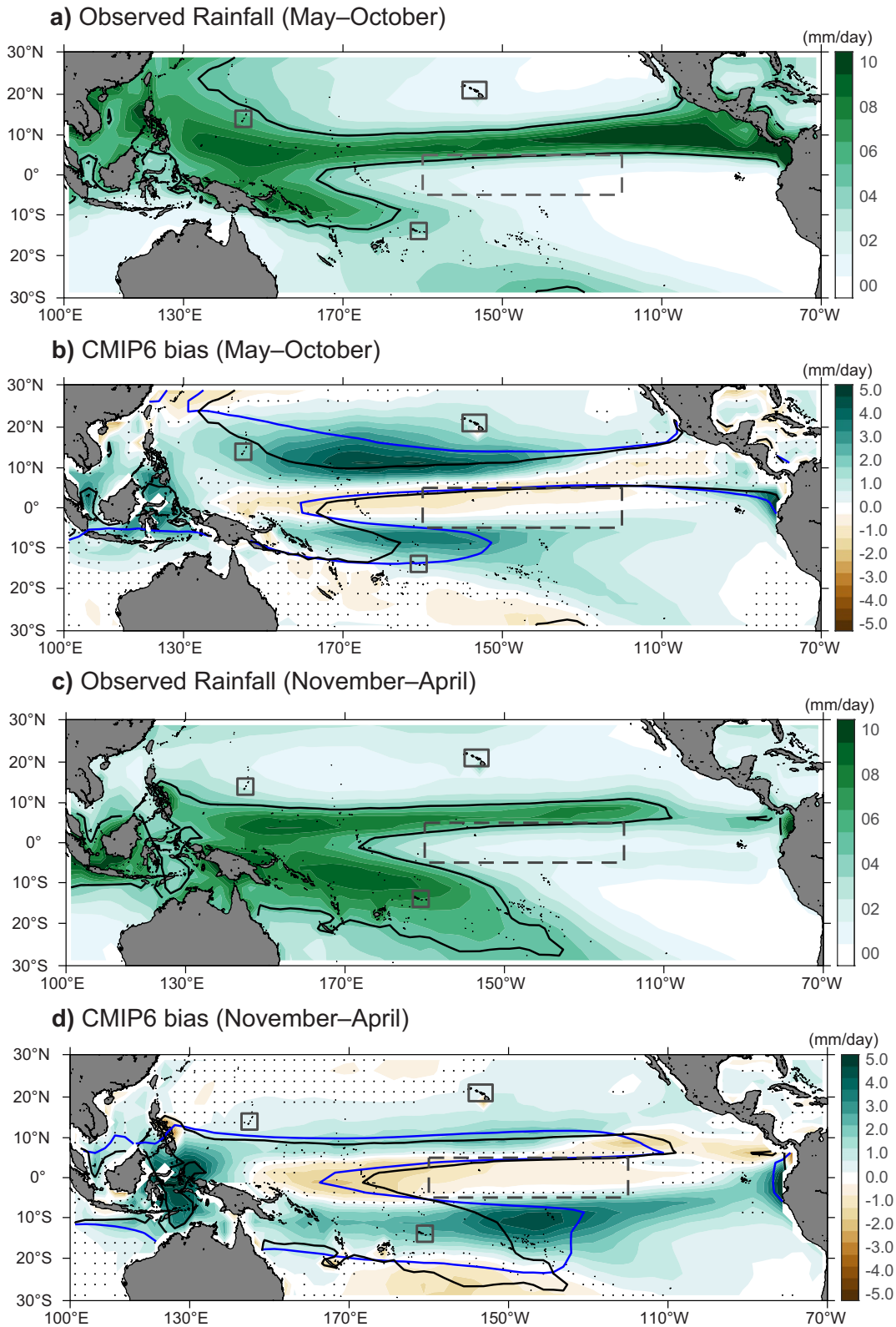

Figure 3. Observed rainfall and CMIP6 bias during 1985–2014 (mm/day, color bars). (a, c) Observed seasonal mean rainfall during May–October and November–April, respectively. (b, d) Multi-model mean rainfall bias for the historical experiment relative to observations during the respective seasons. Contour lines depict the 5 mm/day mean rainfall for the observed (black) and historical (blue) conditions. Black stippling indicates that less than 66% of models agree on the sign of rainfall bias.

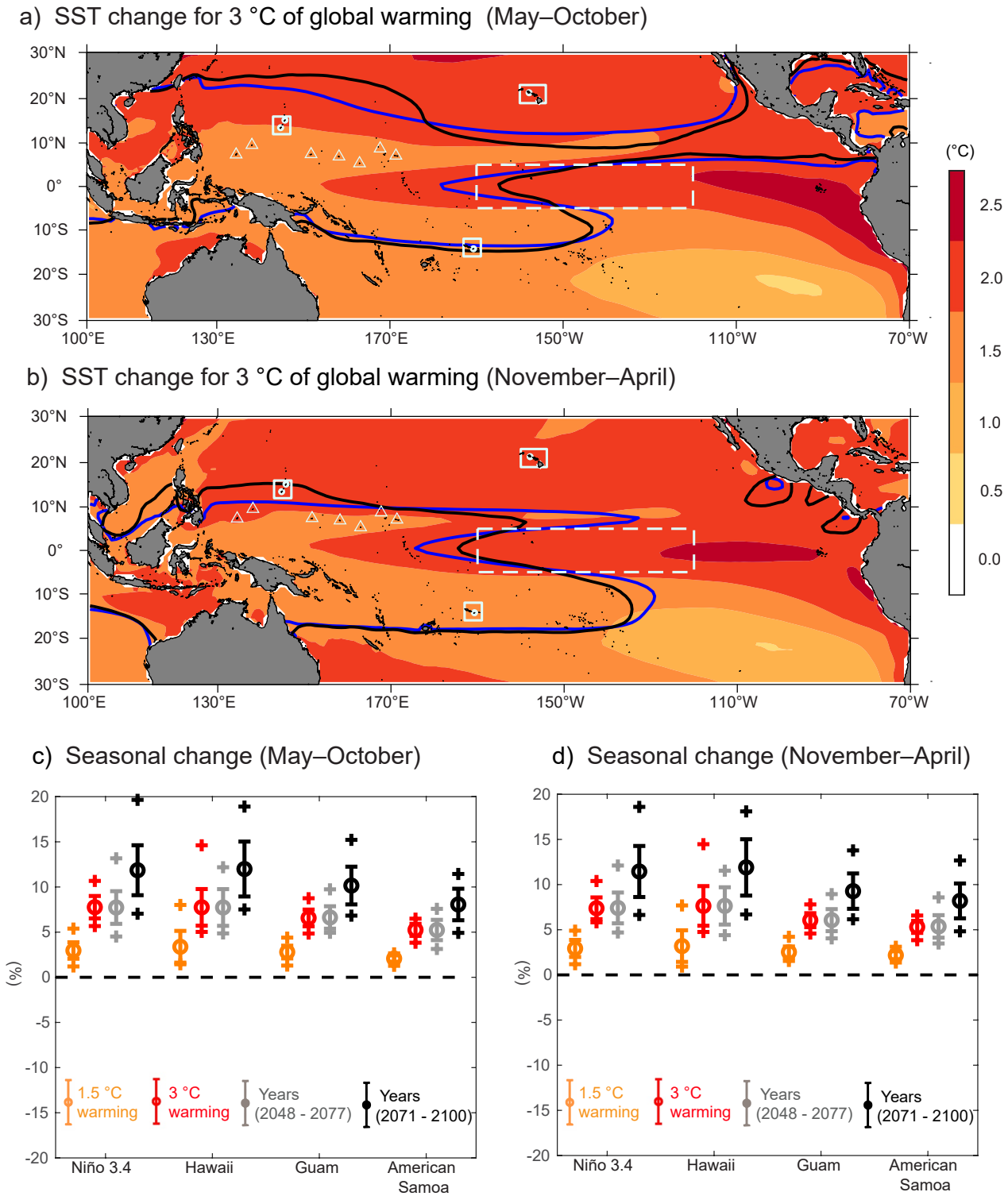

Figure 4. SST seasonal mean changes with respect to 1985–2014 historical conditions. (a, b) Multi-model mean projection for 3°C of global warming (°C, color bar). Two seasons are shown ((a), May–October; (b), November–April). Contour lines depict the 28°C isotherm for the observed (black) and historical (blue) conditions. More than 66% of models agree on the sign of future change everywhere (no stippling). (c, d) Regional SST projections (%) for 1.5°C (yellow) and 3°C (red) of global warming along with projections for fixed time epochs (2048–2077 and 2071–2100; gray and black, respectively). Shown are the multi-model mean (circles), intermodel spread (±1 standard deviation; bars), and model extremes (plus signs).

Table 3
Regional Changes in the Seasonal Mean of SST, Rainfall, and SSH (Annual Mean) for Epochs When the GMST Warms by 1.5°C or 3°C Relative to 1850–1900

Region	Tropical Pacific warming	SST (°C)		Rainfall (mm/day)		SSH (cm)
		November–April	May–October	November–April	May–October	Annual mean
Niño 3.4 (5 °N–5 °S,120–170 °W)	0.7°C	0.8 ± 0.2	0.8 ± 0.3	0.4 ± 0.5	0.3 ± 0.3	Not applicable
	1.8°C	2.1 ± 0.3	2.0 ± 0.3	1.1 ± 0.6	0.9 ± 0.6	Not applicable
Hawaii (19–23 °N, 154–160 °W)	0.7°C	0.8 ± 0.4	0.8 ± 0.4	0.0 ± 0.2	0.0 ± 0.2	15 (13–16)
	1.8°C	1.9 ± 0.5	2.0 ± 0.6	0.0 ± 0.3	0.1 ± 0.3	40 (31–57)
Guam (12–16°N, 143–147 °E)	0.7°C	0.8 ± 0.2	0.7 ± 0.2	0.2 ± 0.4	0.0 ± 0.5	13 (12–14)
	1.8°C	1.8 ± 0.3	1.8 ± 0.2	0.3 ± 0.4	0.5 ± 0.7	36 (28–52)
American Samoa (12–16°S,169–173 °W)	0.7°C	0.6 ± 0.1	0.6 ± 0.1	−0.1 ± 0.5	0.0 ± 0.5	20 (19–22)
	1.8°C	1.5 ± 0.2	1.5 ± 0.2	0.1 ± 0.7	−0.1 ± 0.4	48 (39–63)

Note. With respect to 1985-2014, the equivalent tropical Pacific warming amounts are 0.7 and 1.8°C. Changes of SST, rainfall, and SSH are relative to the more recent historical epoch. For the SST and rainfall changes, the multi-model mean and ±1 standard deviation of the inter-model spread are shown. The SSH changes are based on the local sea level rise projections in Sweet et al. (2022), which we acquired from the Interagency Sea Level Rise Scenario Tool (https://sealevel.nasa.gov/task-force-scenario-tool) for Honolulu (Hawaii), Apra Harbor (Guam), and Pago Pago (American Samoa). Sea level rise projections (Intermediate scenario; ranges are determined by the Intermediate Low and Intermediate High scenarios) are cross-referenced to the nearest decades when 1.5 or 3°C of global warming occurs in the mean number of models for the SSP5-8.5 experiment (i.e., the 2030's and 2060's, respectively).

(Figure 1a). As expected, the GMST warming rate is greater for future simulations prescribed with higher radiative forcing amounts (i.e., comparing the SSP2-4.5 and SSP5-8.5 experiments in Figure 1a). For all models, the SSP5-8.5 experiment warms faster than SSP2-4.5, which on average the GMST reaches 4.8°C (compared to 2.9°C) by 2071–2100. The intermodel spread, for each experiment, contributes even more uncertainty to the warming projection. By 2100, some models in the SSP5-8.5 experiment project global warming of more than 7°C and others are closer to 4°C, which is a range that exceeds the uncertainty between the multi-model averages of the SSP2-4.5 and SSP5-8.5 changes.

The intermodel spread of when global warming amounts will be reached is also large. Figure 1c shows the number of models that reach the 1.5°C and 3°C GMST warming amounts during each decade. For the SSP5-8.5 projection, the multi-model average is for 1.5°C of global warming to occur around 2026 and 3°C of warming around 2063 (with SSP2-4.5 forcing, the lesser warming amount is reached in 2030). As we noted, the intermodel spread is large even considering the same radiative forcing (some models in the SSP5-8.5 experiment warm by 3°C as soon as the 2040s and one model as late as the 2090s); and the distribution of when each model reaches 3°C of global warming is well correlated with the intermodel spread of ECS and TCR values (Figure 1b; see also Meehl et al., 2020).

Assessment of the SSP5-8.5 experiment reveals pronounced spatial differences in which regions of the tropical Pacific warm fastest during the 21st century (Figure 4). These SST changes are determined based on GMST warming with respect to 1850–1900, but are shown with respect to the recent historical epoch (i.e., 3°C of global warming since preindustrial levels is equivalent to 1.8°C of additional warming after 1985–2014 in the tropical Pacific; see Table 2 for warming amounts with respect to each epoch and region). In general, the CMIP6 future projection shows an expanded western Pacific warm pool, and a diminished zonal SST gradient near the equator, which are warming characteristics consistent with projections using prior generations of climate models (e.g., Power et al., 2021). Compared to the tropical Pacific average warming amount of 1.8°C, warming is greater (faster) near and east of the historical 28°C isotherm, such as in the Niño 3.4 region (Figure 4 and Table 3). Since there are not any times of widespread tropical Pacific or global cooling during the SSP5-8.5 experiment (Figure 1a), places that warm more than 1.8°C in this analysis must have a faster warming rate compared to elsewhere (e.g., comparing the SST change in the equatorial eastern Pacific vs. the subtropical south-eastern Pacific). In contrast to the diminished future SST gradient along the equator, the zonal SST gradient poleward of the SPCZ is projected to strengthen (i.e., at 25°S, warming is faster near Australia compared to in most of the south-eastern Pacific). Of the island regions that we assessed, relative to when the tropical Pacific warms by 1.8°C, the warming around Hawaii is greater, Guam is average, and American Samoa is less (Table 3; Table S1 in Supporting Information S1 lists seasonal climate changes for other regions in the USAPI). Overall, the warming pattern, which

is a characteristic of all the regionally different warming rates, will alter somewhat the orientation and seasonal evolution of the future SST pattern.

3.3. Future Seasonal and Annual Cycle Changes in the Climate

We now consider the tropical Pacific climate response to global warming, and specifically assess future changes in the rainfall and SSH patterns. Whereas the future SST projections revealed only subtle differences between the two seasons that we examined (Figures 4a and 4b), here we will explore seasonal differences in the rainfall changes. We will also examine the annual cycle of rainfall, as well as of the SST and SSH variables, using both observations and the CMIP6 experiments. We will thus describe the future changes to the seasonal mean climate (affecting rainfall) and the annual cycle ranges (for each of the variables). Our focus is on describing the climate changes likely to occur when the 3°C global warming amount is reached, and also comparing these changes to the effects of only 1.5°C of warming.

3.3.1. Seasonal Mean Rainfall Changes

Figures 5a and 5b show the seasonal mean rainfall changes for when the GMST warms by 3°C since preindustrial levels. During both seasons that we assessed (i.e., May–October and November–April, or the times centered on boreal summer and winter), there are consistent features in the rainfall changes. Throughout the year, the greatest increases in rainfall are projected near the equator. Drying is projected to occur in some adjacent regions, such as within the eastern part of the observed ITCZ (especially during May–October in the area enclosed by the 5 mm/day rainfall contour near Central America; Figure 5a), and also near the SPCZ eastern boundary in CMIP6 (greatest drying is during November–April; Figure 5b). In these regions and seasons, the drying projections are mostly consistent across models (i.e., no stippling). In all of the remaining future change maps, two compounding layers of stippling are used to indicate uncertainty across models: either black where there is poor agreement on the sign of projections (but perhaps many near-zero changes), or another color where most models also have large changes that differ in sign (e.g., the red stippling in Figures 5a and 5b; uncertainty thresholds are described in the figure captions).

The CMIP6 rainfall projections (Figure 5) are similar to the changes reported in prior climate modeling assessments (e.g., Christensen et al., 2013). In general, the pattern of rainfall change is consistent with the SST projection (see Figures 4a and 4b and Section 3.2) in such a way that places with faster (slower) warming than the basin-wide trend are likely to become wetter (dryer). The projected increase in rainfall near the equator and drying in the eastern part of the simulated SPCZ are examples of this pattern, which follows the so-called "warmer-gets-wetter" climate-change mechanism (Chadwick et al., 2013). We also note that the pattern of rainfall changes for 3°C of global warming (Figures 5a and 5b) is similar to the late 21st-century projection of the SSP5-8.5 experiment (Figure S2 in Supporting Information S1), except that the latter changes are typically larger (i.e., either becoming wetter or drier), which is presumably because additional warming is projected by 2100 (Figure 1a). The exceptions to where the rainfall change increases with time, and hence more greenhouse warming in the SSP5-8.5 experiment, are mostly in regions where the models substantially disagree about the sign of future rainfall changes (i.e., in the red stippled areas of the maps).

Seasonal differences in the rainfall projections are more distinct (i.e., the differences between Figures 5a and 5b), compared to what we noted for SST (Figures 4a and 4b). The largest rainfall increases mostly occur in the summer hemisphere (i.e., more rainfall in the NH during May–October such as around Guam and Hawaii, and in the SH during November–April such as around American Samoa). However, for the Niño 3.4 region during both halves of the year, the multi-model mean projection is to become about 75% wetter with 3°C of global warming (Figures 5c and 5d). For the area around Guam, the monsoonal wet season is projected to become wetter (Figure 5a), with the multi-model mean percentage change being about a 10% increase during May–October for 3°C of global warming (Figure 5c; the increase is smaller for 1.5°C of warming). The absolute change in the Guam rainfall is much smaller during November–April (Figure 5b; see also Table 3); however, the percentage changes are larger on average during the dry season (Figure 5d) compared to the wet season (Figure 5c). Around Hawaii, the largest rainfall change in absolute (0.1 ± 0.3 mm/day; Table 3) and percentage terms (15% increase; Figure 5c) is during May–October. During the opposite season (i.e., winter), there is no consensus whether the future will be wetter or drier (the intermodel range of projections is centered on zero and exceeds ±20%; Figure 5d). We note that boreal summer is the local dry season in Hawaii because it is an unusual tropical location with most of the rainfall

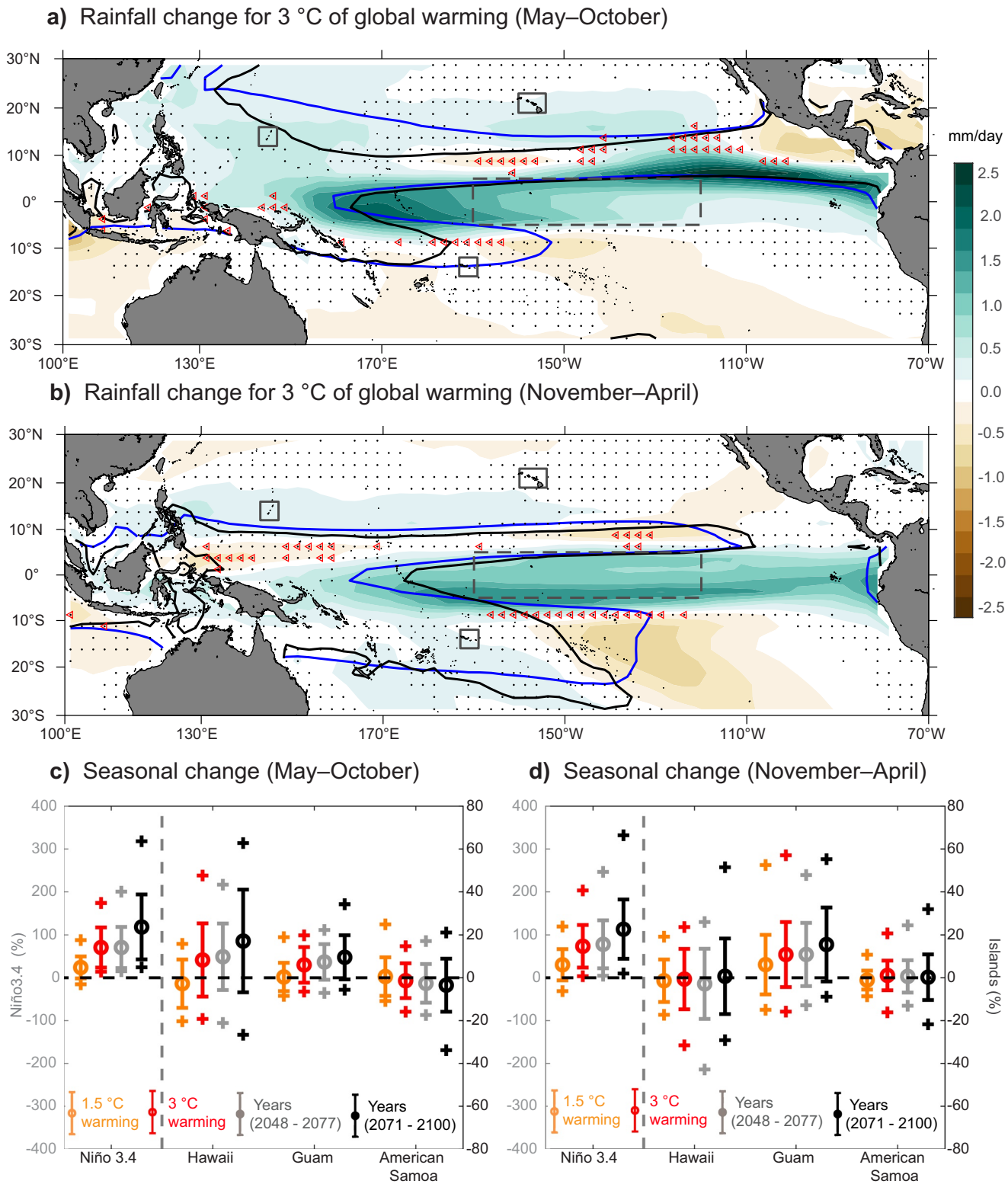

Figure 5. Rainfall seasonal mean changes with respect to 1985–2014 historical conditions. (a, b) Multi-model mean projection for 3°C of global warming (mm/day, color bar). Two seasons are shown ((a), May–October; (b), November–April). Contour lines depict the 5 mm/day seasonal mean rainfall for the observed (black) and historical (blue) conditions. Black stippling indicates where less than 66% of models agree on the sign of future change and red stippling indicates where in those places more than 66% of models project large changes (exceeding ±0.5 mm/day). (c, d) Regional rainfall projections (%; left axes, Niño 3.4; right axes, islands) for 1.5°C (yellow) and 3°C (red) of global warming along with projections for fixed time epochs (2048–2077 and 2071–2100; gray and black, respectively). Shown are the multi-model mean (circles), intermodel spread (±1 standard deviation; bars), and model extremes (plus signs).

occurring in the winter (Giambelluca et al., 2013). Around American Samoa, there is a broad area of uncertainty about the future rainfall change, which encompasses most of the SPCZ region and is present during both seasons (see black and red stippling in Figures 5a and 5b). Some models in the CMIP6 ensemble suggest the possibility of the wet season for American Samoa becoming more than 20% dryer or wetter by the end of the 21st century, although the multi-model mean projection is for almost no change of rainfall during both seasons (Figures 5c and 5d and Table 3). The uncertainty increases with more warming (i.e., comparing the model spread for 1.5°C or 3°C of global warming). Considering each of the regions, and both seasons, the uncertainty typically increases from the mid-to-late 21st century (indicated by gray and black colors in Figures 5c and 5d), although there is no clear reduction in uncertainty for the analysis based on using the 3°C global warming epoch versus the time when that amount of warming occurs in most models (2048–2077; i.e., there are similar spans of the red and gray bars as well as the respective outliers). Any seasonal asymmetry in the future rainfall absolute changes for these regions would result in pronounced changes to the climatological annual cycle.

3.3.2. Annual Cycle Changes

The annual cycle is the largest mode of climate variability observed in much of the tropical Pacific. In many places, the yearly range in SST, rainfall, and/or SSH exceeds even the interannual variability associated with ENSO (Figures S3–S5 in Supporting Information S1 show spatial patterns of the annual cycle ranges and interannual standard deviations for each variable, as observed and also compared to the CMIP6 historical experiment). Around Hawaii, for example, the yearly SST range is about 3°C (coolest in March and warmest in September; Figure 6a), whereas the interannual standard deviation of SST is only about 0.5°C in almost all of the tropical Pacific, except for the near-equatorial region most directly influenced by ENSO (i.e., around the Niño 3.4 region; Figure S3 in Supporting Information S1). For rainfall and SSH, the annual ranges are likewise substantial in many places (e.g., Guam experiences yearly ranges of about 8 mm/day in rainfall and 12 cm in SSH; Figures 6b and 6c).

In many parts of the tropical Pacific, the 12-month evolution of regional SST (Figure 6a) is nearly in phase with the amount of monthly rainfall experienced (Figure 6b). Guam and American Samoa are examples of the general synchronization between the months of warmer SST (exceeding 29°C) and greatest rainfall in the respective regions (again, note the opposite wet seasons in most of the northern and southern tropical Pacific). Hawaii is an exception, as we noted, in that most of the local rainfall is observed during the cooler months (i.e., during December–March, when the SST is around 24°C). Timing of the peak in the SSH annual cycle (Figure 6c) also shares similarities to SST, at least in several parts of the tropical Pacific (e.g., around Hawaii and Guam, but not American Samoa nor in the Niño 3.4 region). Since the SSH is influenced by the entire ocean density structure (i.e., primarily thermosteric sea level variability; e.g., Widlansky et al., 2020), it is not unexpected that the observed SSH and SST annual cycles are out of phase in some places, such as in the Niño 3.4 region, where the subsurface temperature variability is large and sometimes strikingly different from the SST (Zhao et al., 2021).

CMIP6 models generally resolve the observed annual cycles of SST, rainfall, and SSH during the historical experiment (i.e., comparing the black and blue lines in Figures 6a–6c); however, there are several notable biases. Hawaii is again an exception where most of the simulated rainfall occurs too early in the year compared to observations (i.e., during September and October, when the regional SST is actually warmest; about 27°C), instead of during the winter wet season. In Guam and American Samoa, we also note that both the SST and rainfall annual cycles are somewhat too large compared to the observations, which is consistent with the seasonal differences seen in the maps of CMIP6 bias (Figures 2 and 3). The SSH annual cycle in CMIP6 closely matches the Guam observations, and resembles the Hawaii observations, but is almost completely out of phase with observations around American Samoa and in the Niño 3.4 region, at least in a multi-model mean sense.

The CMIP6 future projections indicate a general increase of the climatological annual cycles for the studied variables (SST, rainfall, and SSH), including mostly increases for the island regions that we assessed (Figure 6). Exceptions do exist, however, such as the almost no change of the SST annual cycle projected for Guam (Figure 6a). The projection of increased rainfall annual cycles is much more consistent across regions (Figure 6b), which is generally because the future wet seasons become wetter and dry season changes are smaller (e.g., increased rainfall in Guam is mostly during May–October; see also Figure 5). In contrast to the robust increase in the rainfall annual cycle ranges, the SSH projections are more inconsistent across regions (i.e., increasing in Hawaii and Guam, decreasing in American Samoa, and remaining almost unchanged in the Niño 3.4 region; Figure 6c).

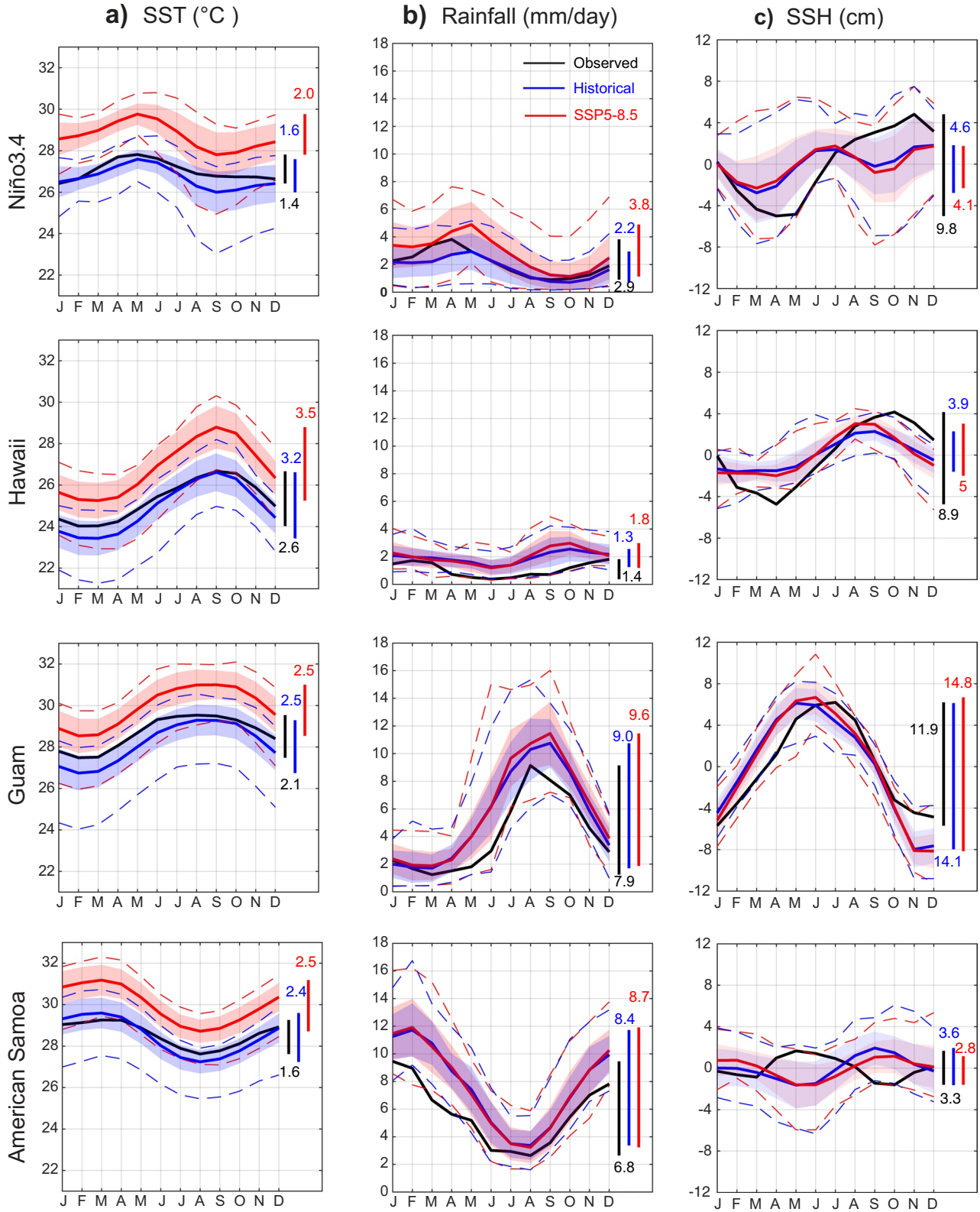

Figure 6. Annual cycle projected changes for 3°C of global warming. (a–c) Regional annual cycles of SST, rainfall, and SSH, respectively, for observations (black), historical (blue), and future warming (red). SSH annual cycles are normalized to have a mean of zero (i.e., sea level rise is not included). The multi-model mean, intermodel spread (±1 standard deviation), and model extremes are indicated by solid lines, shading, and dashed lines, respectively. Vertical lines indicate the multi-model mean annual cycle ranges in the units of the respective column.

Considering the spatial patterns of the CMIP6 future projections in the annual cycle ranges for each of SST, rainfall, and SSH (Figures 7a, 8a and 9a, respectively) reveals some common characteristics about the changes. For SST, the annual cycle is projected to increase nearly everywhere, with Guam and most of the tropical north-western Pacific being one of only two regions where there are future decreases. On a percentage basis, however, the amplitude changes are small for Guam (Figure 7c). The other region of a future decrease in the SST annual cycle is in the far eastern part of the equatorial Pacific (i.e., east of the Niño 3.4 region). For the Niño 3.4 region itself, the projected increase of the SST annual cycle is the largest change among all of the regions that we assessed (i.e., almost a 20% increase for 3°C of global warming as shown in Figure 7c; see also Table 4 and Table S2 in Supporting Information S1 for the absolute variability changes in each region).

For the rainfall annual cycle changes, the CMIP6 future projection is likewise for increases nearly everywhere with mostly strong model agreement (Figures 8a and 8c). The greatest increase in the rainfall annual cycle is projected for the equatorial central and eastern Pacific, where thermodynamic changes may explain the increase (Marvel et al., 2017). There are only a few regions with either a projected decrease in the rainfall annual cycle, or appreciable model disagreement (indicated by red stippling in Figure 8a), which generally match the places of future drying during the local wet season (e.g., in the eastern ITCZ region during May–October as well as near the SPCZ eastern boundary during November–April; Figures 5a and 5b). The projected decrease of the rainfall annual cycle in the subtropics of the south-eastern Pacific is consistent with the expansion of the Hadley circulation, which is a dynamic response to greater future rainfall and associated convection near the equator (Marvel et al., 2017). The equatorial western Pacific is a region of intermodel uncertainty about the future change to the rainfall annual cycle. We note that the equatorial western Pacific is a region where the CMIP6 historical annual cycle of rainfall is too large compared to observations (Figure S4 in Supporting Information S1), which perhaps contributes to uncertainty about the future change there.

The SSH annual cycle changes (Figures 9a and 9c) are more uncertain, at least on a regional basis, compared to SST and rainfall changes. Whereas the SSH annual cycle is projected to increase in the tropical Pacific overall (the domain average change is 6 ± 3%; multi-model mean and ±1 standard deviation of intermodel spread), there are many regions of large intermodel uncertainty about the future change (indicated by green stippling in Figure 9a). The projection of increased SSH annual cycle ranges is most widespread and robust across models in the northern tropical Pacific (i.e., non-stippled in Figure 9a), including around Hawaii (20% multi-model mean increase for 3°C of global warming; Figure 9c). There is more uncertainty around American Samoa and in parts of the Niño 3.4 region. Many places with large uncertainty also have small observed annual cycles of SSH and/or large historical biases in CMIP6 (see Figure S5 in Supporting Information S1). As we noted, American Samoa and the Niño 3.4 are where the CMIP6 historical annual cycle of SSH is out-of-phase with observations, at least in some models (Figure 6c). In the Niño 3.4 region, the future change of the SSH annual cycle is uncertain (Figure 9c), especially compared to the more robust increases in the annual range of both SST and rainfall (Figures 7c and 8c, respectively).

3.4. Future Interannual Variability Changes

Occurrence of ENSO events is associated with most of the interannual variability in the tropical Pacific, and this variability is projected to respond in various ways to ongoing climate change (McPhaden et al., 2020). We describe the amount of interannual variability by measuring the standard deviation of monthly anomalies for SST, rainfall, or SSH (see Section 2.2 for the full methodology). Here, we first briefly assess the observations and biases of interannual variability, then describe similarities or differences between the projected future changes for each of the variables.

The largest interannual variability of SST is observed in a narrow band of the equatorial central and eastern Pacific (i.e., bounded by 5°N/S and generally within or east of the Niño 3.4 region; Figure S3 in Supporting Information S1). For rainfall, the pattern of interannual variability is more extensive in area, with the largest variability occurring mostly within or adjacent to the major rainfall bands depicted in the seasonal mean (i.e., comparing the interannual variability in Figure S4 in Supporting Information S1 with the boundaries of heavy rainfall in Figure 3). The SSH variability is also extensive, especially in the tropical western Pacific, throughout the equatorial latitudes, and near the North and South American Coasts (Figure S5 in Supporting Information S1). The widespread interannual variability of rainfall and SSH, which is in contrast to the more equatorially constrained

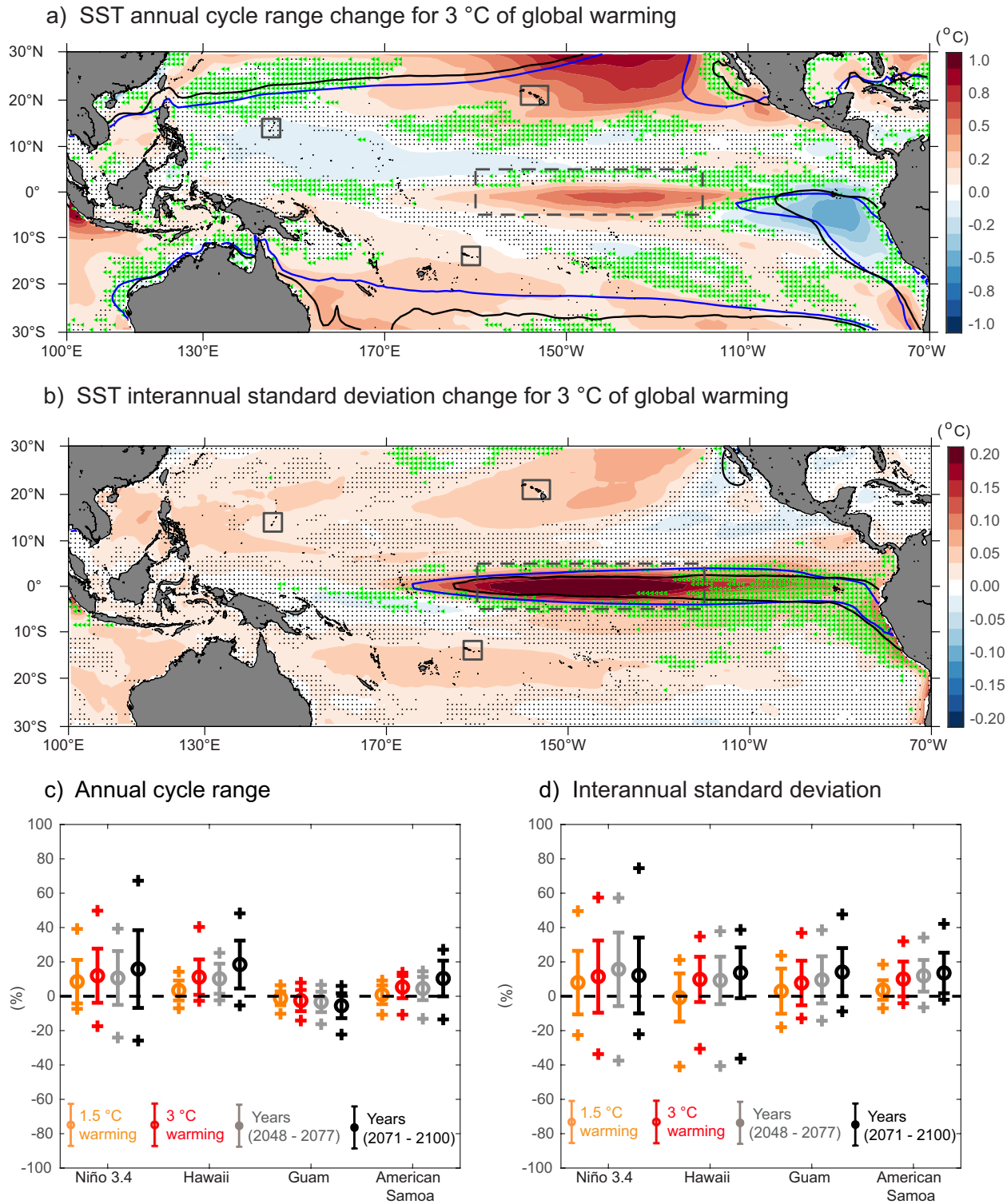

Figure 7. SST variability changes. (a, b) Multi-model mean projection for 3°C of global warming of the annual cycle and interannual variability changes, respectively (°C, color bars). Contour lines depict the annual cycle range of 5°C (a) and interannual standard deviation of 1°C (b) for the observed (black) and historical (blue) conditions. Black stippling indicates where less than 66% of models agree on the sign of future change and green stippling indicates where in those regions more than 66% of models project large changes ((a), annual cycle change exceeding ±0.125°C; (b), interannual standard deviation change exceeding ±0.05°C). (c, d) Regional projections (%) for the annual cycle range and interannual standard deviation, respectively, for 1.5°C (yellow) and 3°C (red) of global warming along with projections for fixed time epochs (2048–2077 and 2071–2100; gray and black, respectively). Shown are the multi-model mean (circles), intermodel spread (±1 standard deviation; bars), and model extremes (plus signs).

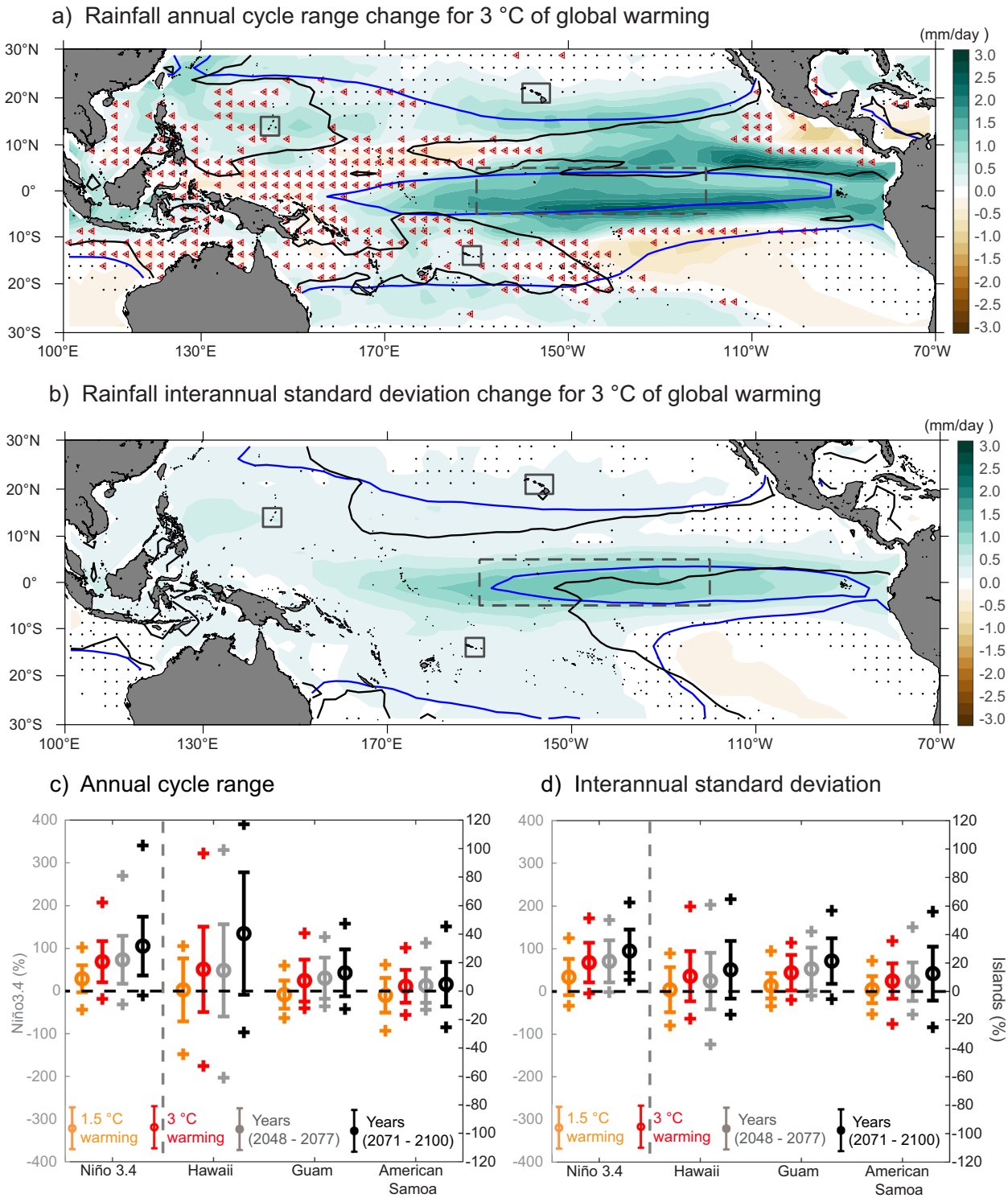

Figure 8. Rainfall variability changes. (a, b) Multi-model mean projection for 3°C of global warming of the annual cycle and interannual variability changes, respectively (mm/day, color bar). Contour lines depict the annual cycle range of 5 mm/day (a) and interannual standard deviation of 2 mm/day (b) for the observed (black) and historical (blue) conditions. Black stippling indicates where less than 66% of models agree on the sign of future change and red stippling indicates where in those regions more than 66% of models project large changes ((a), annual cycle change exceeding ±0.25 mm/day; (b), interannual standard deviation change exceeding ±0.25 mm/day). (c, d) Regional projections (%; left axes, Niño 3.4; right axes, islands) for the annual cycle range and interannual standard deviation, respectively, for 1.5°C (yellow) and 3°C (red) global warming along with projections for fixed time epochs (2048–2077 and 2071–2100; gray and black, respectively). Shown are the multi-model mean (circles), intermodel spread (±1 standard deviation; bars), and model extremes (plus signs).

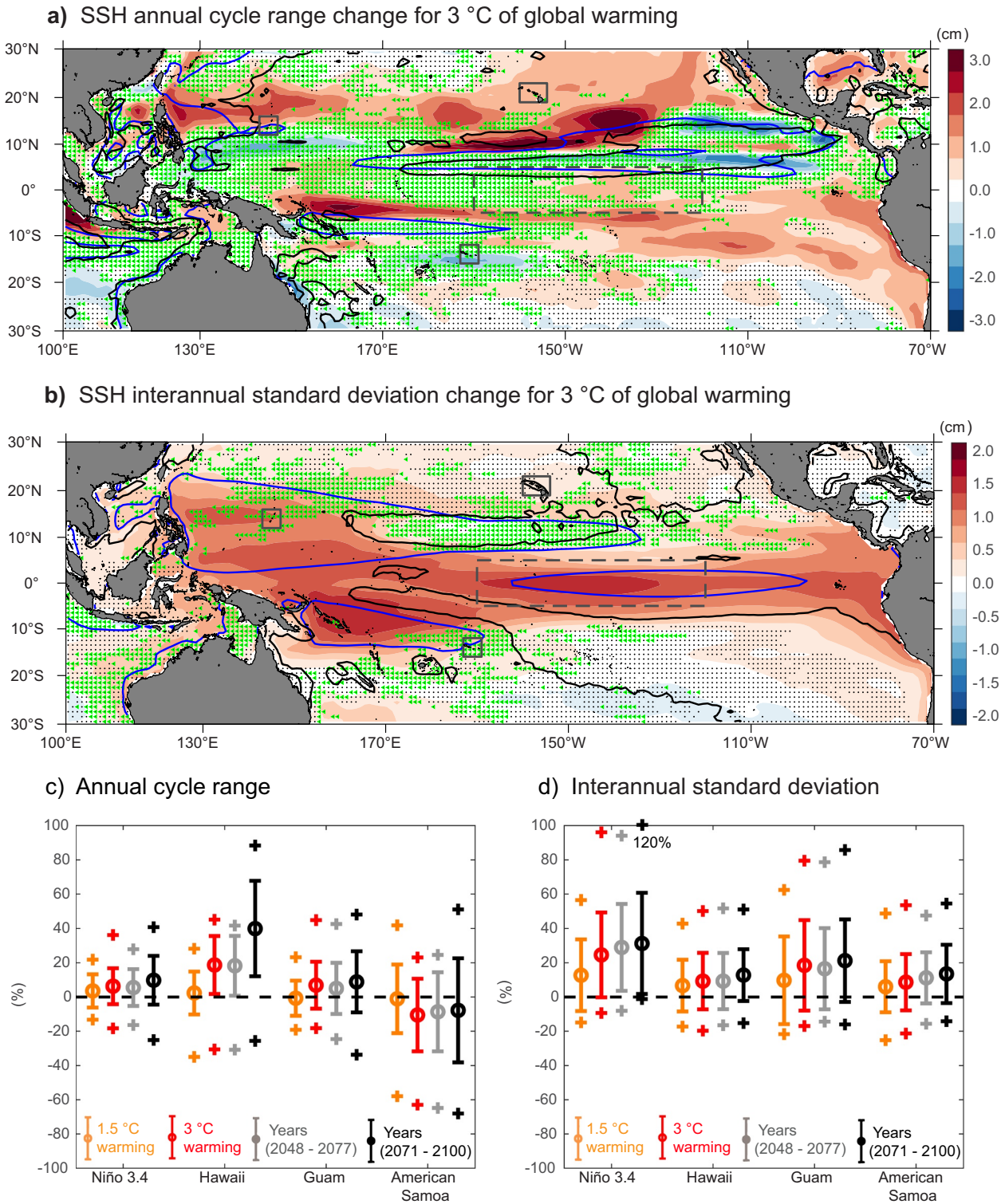

Figure 9. SSH variability changes. (a, b) Multi-model mean projection for 3°C of global warming of the annual cycle and interannual variability changes, respectively (cm, color bar). Contour lines depict the annual cycle range of 15 cm (a) and interannual standard deviation of 5 cm (b) for the observed (black) and historical (blue) conditions. Black stippling indicates where less than 66% of models agree on the sign of future change and green stippling indicates where in those regions more than 66% of models project large changes ((a), annual cycle change exceeding ±0.5 cm; (b), interannual standard deviation change exceeding ±0.25 cm). (c, d) Regional projections (%) for the annual cycle range and interannual standard deviation, respectively, for 1.5°C (yellow) and 3°C (red) of global warming along with projections for fixed time epochs (2048–2077 and 2071–2100; gray and black, respectively). Shown are the multi-model mean (circles), intermodel spread (±1 standard deviation; bars), and model extremes (plus signs).

Table 4
Similar to Table 3, But for Regional Changes in the Annual Cycle (Range) and Interannual Variability (Standard Deviation) of SST, Rainfall, and SSH

		SST (°C)		Rainfall (mm/day)		SSH (cm)	
Region	GMST warming	Annual cycle	Interannual variability	Annual cycle	Interannual variability	Annual cycle	Interannual variability
Niño 3.4 (5 °N–5 °S, 120–170 °W)	1.5°C	0.2 ± 0.3	0.09 ± 0.21	0.7 ± 0.7	0.6 ± 0.7	0.4 ± 1.0	0.6 ± 1.0
	3°C	0.3 ± 0.3	0.13 ± 0.24	1.7 ± 1.1	1.1 ± 0.7	0.6 ± 1.1	1.2 ± 1.2
Hawaii (19–23 °N, 154–160 °W)	1.5°C	0.1 ± 0.2	0.00 ± 0.07	0.0 ± 0.4	0.0 ± 0.2	0.1 ± 0.7	0.2 ± 0.4
	3°C	0.4 ± 0.3	0.05 ± 0.06	0.3 ± 0.6	0.2 ± 0.3	1.0 ± 0.9	0.3 ± 0.5
Guam (12–16 °N, 143–147 °E)	1.5°C	0.0 ± 0.1	0.01 ± 0.06	−0.2 ± 1.0	0.1 ± 0.3	−0.1 ± 1.5	0.6 ± 1.5
	3°C	−0.1 ± 0.2	0.03 ± 0.06	0.7 ± 1.5	0.4 ± 0.4	1.0 ± 2.0	1.1 ± 1.6
American Samoa (12–16 °S,169–173 °W)	1.5°C	0.0 ± 0.1	0.02 ± 0.02	−0.3 ± 1.1	0.0 ± 0.3	−0.1 ± 1.4	0.3 ± 0.7
	3°C	0.1 ± 0.2	0.04 ± 0.04	0.7 ± 1.1	0.2 ± 0.4	−0.7 ± 1.5	0.4 ± 0.8

Note. The regional climate changes are relative to the recent historical epoch (1985–2014), and are for GMST warming amounts of either 1.5°C or 3°C with respect to the early historical epoch (1850–1900).

SST variability, is indicative of the local and remote influences of ENSO and other modes of variability on the climate (Lorrey & Fauchereau, 2018).

Compared to the observed interannual variability of SST, the CMIP6 historical standard deviation is somewhat too large throughout most of the tropical Pacific (Figure S3 in Supporting Information S1). There are only a couple of localized exceptions where the simulated variability is smaller than observed; in particular, near the North and South American Coasts. The largest positive bias in CMIP6 is near the eastern part of the Niño 3.4 region, where most of the observed variability occurs. Interestingly, the CMIP6 rainfall interannual variability is much smaller than observed in the Niño 3.4 region (Figure S4 in Supporting Information S1), which is also where the climate models are too dry overall (especially during November–April; Figure 3d). In most other parts of the tropical Pacific, the rainfall interannual variability in CMIP6 is larger than observed. For the SSH interannual variability (Figure S5 in Supporting Information S1), CMIP6 has a low bias nearly everywhere. The deficiency is largest in the subtropics where the model resolutions are too coarse (Table 1) to resolve oceanic processes necessary to explain much of the observed variability (e.g., associated with mesoscale eddies around Hawaii, which perhaps interact with ENSO; Long et al., 2020).

With future global warming, the SST interannual variability is projected to increase throughout most of the tropical Pacific, and especially in the equatorial central Pacific (Figure 7b). The largest projected increase in variability is in the Niño 3.4 region (an 11% change of the standard deviation for 3°C of global warming; Figure 7d). We note that intermodel spread is large in the equatorial eastern Pacific (green stippling in Figure 7b), which is indicative of substantial uncertainty about how ENSO will change. For 3°C of global warming, the intermodel spread of the Niño 3.4 standard deviation change is from almost a 60% increase to nearly a 40% decrease (Figure 7d). For the time-based analyses of SST interannual variability during the mid- and late-21st century, we notice no clear difference in the amount of uncertainty between epochs (or for comparing either time to when 3°C of global warming occurs), although the intermodel spreads are always smallest for changes associated with the 1.5°C warming amount (Figure 7d). Specifically, for the island regions that we assessed, there is more agreement across models that the SST interannual variability will either increase or remain unchanged with future warming (i.e., these areas are completely non-stippled in Figure 7b). However, the changes for Hawaii, Guam, and American Samoa are much smaller in absolute units compared to in the Niño 3.4 region (Table 4).

Rainfall interannual variability is likewise projected to increase throughout most of the tropical Pacific, with the largest change in the Niño 3.4 region (Figure 8b). However, unlike the uncertainty that we noted for the change in SST interannual variability in the equatorial eastern Pacific, the CMIP6 models are in much stronger agreement about the projected increase in rainfall variability (red stippling is non-existent in Figure 8b). In fact, the multimodel mean percentage increase in Niño 3.4 rainfall standard deviation associated with 3°C of global warming is more than six times greater than the change for SST (68% vs. 11%; note the differing *y*-axes in Figures 7d and 8d). Also, the end-of-century increase in the Niño 3.4 rainfall standard deviation (i.e., during 2071–2100) is larger than all of the other changes for when less global warming occurs. Outside of the equatorial Pacific, the projected

changes in the rainfall interannual variability are smaller, but the vast majority of models agree on the future increase in most places. For Hawaii, Guam, and American Samoa, the respective multi-model mean increases for 3°C of global warming are 11%, 13%, and 7%. The nearly basin-wide tendency for the interannual variability of rainfall to increase with future greenhouse warming has been previously reported in climate change assessments (e.g., Yun et al., 2021) and is a manifestation of the atmospheric response to both the increased SST variability in the Niño 3.4 region projected by most models, as well as the mean warming of the tropical Pacific and associated moisture increase (He & Li, 2019; Pendergrass et al., 2017).

The projected change in SSH interannual variability shares many characteristics with the SST and rainfall response to future warming. Overall, the CMIP6 projection is for increased SSH interannual variability throughout the equatorial Pacific, along the North and South American Coasts, and also in the entire tropical western Pacific (i.e., between 20 °N/S and west of the dateline; Figure 9b). The future changes are largest in the places with most of the simulated variability in the historical experiment, such as in the Niño 3.4 region and also around Guam. In both of these regions, the multi-model mean increases are about 20% (Figure 9d). The increased variability around Hawaii and American Samoa is somewhat smaller (i.e., around 10%), and much smaller in absolute units (Table 4). In most of the subtropics (i.e., poleward of 20 °N/S), changes are small or highly uncertain (i.e., many areas of black and green stippling in Figure 9b). The subtropical Pacific is also where the CMIP6 models do not simulate well the observed amount of the SSH variability (Figure S5 in Supporting Information S1). Projected increases in SSH interannual variability noted here are consistent with previous assessments using CMIP5 experiments that found increasing sea level variability associated with more extreme future ENSO events (Widlansky et al., 2015), and also a near-global tendency for the ocean density fluctuations to increase with mean warming (Widlansky et al., 2020). Interestingly, there is intermodel uncertainty in the future change of SST interannual variability in the equatorial eastern Pacific (i.e., green stippling mostly east of the Niño 3.4 region in Figure 7b), but there is no such uncertainty for the projection of increased SSH interannual variability in that region (Figure 9b).

4. Summary and Discussion

We assessed the CMIP6 historical climatology and future changes that are projected to occur in the tropical Pacific for two different global warming amounts likely to be exceeded sometime during the 21st century. Our focus was on the SST, rainfall, and SSH characteristics of the climate, in particular concerning changes to the seasonal mean, annual cycle, or interannual variability. These are climate variables with great societal and ecological relevance around the numerous tropical Pacific Islands and associated coastal environments. Similar to assessments of prior-generation global climate models (e.g., CMIP5), we found the CMIP6 models mostly capable of simulating well the large-scale characteristics of SST, rainfall, and SSH in the tropical Pacific. There are notable biases, however, especially concerning the annual cycles of rainfall (e.g., around Hawaii) and SSH (e.g., around American Samoa and in the Niño 3.4 region). We also found that the CMIP6 projected climate changes are generally similar as have been identified and described using CMIP5 greenhouse warming experiments (e.g., Grose et al., 2014; G. Li et al., 2016; Samanta et al., 2019; Widlansky et al., 2015). There is some uniqueness to the CMIP6 projections, however, as well as our methodology for analyzing the experiments. We briefly summarize the results and then discuss aspects of the study in the context of exploring limitations of the methodology, potential research opportunities, as well as providing information for guiding climate adaptation efforts in the tropical Pacific Islands.

The fastest warming is projected in the equatorial Pacific (Figure 4), especially near and east of the Niño 3.4 region, which is also the area with greatest rainfall increase (Figure 5). The Niño 3.4 region has the largest increase in interannual variability for each of SST (Figure 7b), rainfall (Figure 8b), and SSH (Figure 9b), although most of the tropical Pacific is projected to experience more climate variability in the future. Slower warming is projected for American Samoa and, in that region of the tropical South Pacific, there is no consensus in CMIP6 whether the future will become wetter or drier (Figure 5), which is a similar result to the CMIP5 experiments (Brown, Lengaigne, et al., 2020; Widlansky et al., 2013). Relatively faster warming is projected in the tropical North Pacific, especially around Hawaii. Yet, the future rainfall change remains uncertain there. Around Guam, where the projected warming rate matches the tropical Pacific average, CMIP6 models mostly agree on a wetter future, and with larger annual and interannual variability of rainfall. SSH interannual variability is also projected to increase around Guam.

We note several limitations about the data and methodology that we applied for assessing future climate changes. By defining our model-selection criteria as only dependent on the availability of the necessary variables (GMST, SST, rainfall, and SSH) from the historical and future CMIP6 experiments (Table 1), we created the largest possible ensemble of models. However, the multi-model ensemble consists of several somewhat-related models (primarily those developed by the same institutions), which may skew our assessment of intermodel uncertainty. Furthermore, the spread of future greenhouse warming scenarios in our analysis is limited because we only considered two experiments during the 21st century (i.e., the SSP2-4.5 and SSP5-8.5 scenarios). We also left mostly unanswered what climate changes in the tropical Pacific are likely for future global warming greater than 3°C. However, the end-of-century SSP5-8.5 projections of seasonal rainfall (i.e., during 2071–2100; Figure S2 in Supporting Information S1) showed only subtle differences in which regions become wetter or drier, compared to the changes associated with 3°C of warming (Figure 5).

Our assessment methodology of describing future climate changes as a function of warming amounts, instead of time, is unique for studies of this scope in the tropical Pacific. Motivation for this approach was both to reduce the uncertainty of future projections associated with unknowns about what greenhouse gas radiative forcing scenario will be realized (i.e., which SSP-RCP possibility is most likely to occur?), as well as the large intermodel spread in the climate response to the same radiative forcing (e.g., the spread across models of global warming in 2100 for a particular radiative forcing; Figure 1a). The method was partially successful in that we have provided location-based projections of the most likely regional climate changes for when the GMST warms by 1.5°C or 3°C compared to preindustrial levels, which is approximated by the early historical epoch. Reaching the higher of these warming amounts is likely as soon as mid-century, if the greenhouse radiative forcing continues to increase as quickly as in the SSP5-8.5 scenario (Figure 1c). However, comparing our regional climate change assessment based on 3°C of global warming with the time-based changes that are projected to occur when most models warm by such an amount (i.e., during 2048–2077 in the SSP5-8.5 experiment) did not reveal systematic differences in either the multi-model mean results or a reduction in the intermodel uncertainty (e.g., Figures 5c and 5d). Instead, the comparison suggests an interchangeability between warming-based and time-based climate change assessments.

We revealed many remaining uncertainties inherent to the current generation of climate models, which are distinct from the variety of warming rates projected by each model because of their differing greenhouse warming sensitivities (Meehl et al., 2020; Zelinka et al., 2020). These climate change uncertainties for the same amount of future warming are manifested by the intermodel spreads of each projection, which we indicated throughout the assessment. Using two layers of stippling on maps (e.g., Figures 5a and 5b), we showed where many models disagree on the sign of future change; and, within those areas, where at least a majority of models project relatively large changes. Thus, we described where models either mostly agree on the sign of future changes (indicated by no stippling), disagree on the sign but have mostly small changes (black stippling), or have a large disagreement about the sign (colored stippling). In terms of absolute rainfall changes (i.e., mm/day averaged over a season), the analysis distinguishes between regions where there is a robust projection of almost no change (i.e., white shading with either no stippling or black stippling on the contour maps) versus a multi-model mean projection of no change that is highly uncertain because the intermodel spread is large (i.e., red stippling). Such a layered categorization of the climate change uncertainty (e.g., concerning seasonal rainfall changes) could be especially relevant to guiding policy-making decisions related to climate change adaptation.

Description of intermodel uncertainties also provides insight about the likelihood of future changes to ENSO and interannual variability in general. Assessment of the SST standard deviation response to 3°C of global warming (Figure 7b) revealed an overall increase in interannual variability throughout the tropical Pacific, which is largest near the equatorial central Pacific (i.e., in the Niño 3.4 region). However, there are stark regional differences in the intermodel uncertainty of how SST interannual variability will change. Whereas the projection of increased SST variability in the Niño 3.4 region is somewhat consistent across CMIP6 models, and the local change is generally greater for more warming (Figure 7d), there is no consensus in the equatorial far-eastern Pacific where the majority of models greatly disagree (i.e., indicated by green stippling in Figure 7b). This regionally dependent uncertainty about the SST interannual variability change and, especially, its association with how ENSO will respond to future global warming, remains an active research topic (e.g., Beobide-Arsuaga et al., 2021; Cai et al., 2021; Fredriksen et al., 2020).

Noting that the Niño 3.4 region is where some of the greatest intermodel differences occur for the SSH annual cycle, as well as the previously explored linkages between the annual cycle and ENSO changes (Brown, Brierley, et al., 2020; Karamperidou et al., 2020; Timmermann et al., 2004), suggests that more comprehensive analysis of the ocean density structure and sea levels are warranted. The SSH annual cycle in the Niño 3.4 region is poorly resolved in CMIP6, with at least some of the models being almost completely out of phase compared to observations (Figure 6c). This SSH bias is in stark contrast with the well-resolved SST annual cycle in the Niño 3.4 region (Figure 6a). Furthermore, there is weak intermodel consensus on whether the future SSH annual cycle will increase in the Niño 3.4 region (Figure 9c). However, the overall tendency is for increasing SSH variability in the tropical Pacific (Figure 9a), which is partially associated with the thermodynamic response of ocean density fluctuations in response to warming seawater (i.e., the nonlinear equation of state will cause greater density variability to occur even if the annual cycle or interannual variability of the ocean temperature remains unchanged; Widlansky et al., 2020).

Besides the SSH annual cycle discrepancies, we reported several other biases in CMIP6 that are mostly consistent with prior-generation models. In the historical experiment, the tropical Pacific climate continues to be much too wet overall compared to the rainfall observations that we used (i.e., GPCP version 2.3; Figure 3). However, there are large uncertainties in the observed rainfall among different products, especially over the ocean (e.g., Roca et al., 2019), which limits our confidence to quantify the CMIP6 rainfall biases using a comparison to only one product. It remains unclear how climate model biases in general affect the future projections (e.g., do regions that are too wet in the historical experiment have an unrealistic increase in future rainfall?), despite past efforts to investigate this type of question (e.g., using bias-correction experiments to study future rainfall changes around the SPCZ; Widlansky et al., 2013). Perhaps most troubling about the CMIP6 simulation of rainfall is that the historical biases are larger than the projected changes in many places (i.e., comparing Figures 3 and 5 for each of the regions around Hawaii, Guam, and American Samoa).

Another fundamental limitation of using CMIP6 experiments to assess climate change projections for tropical Pacific Islands is due to the model spatial resolutions (Table 1) being too coarse to resolve complex atmospheric flows and/or oceanic circulations that exist, especially around some of the higher islands. Next-generation global coupled climate models with much finer spatial resolutions are clearly needed, although it remains unknown how best to develop, test, and utilize such models. Furthermore, regional downscaling approaches using statistical or dynamical models are already commonly applied to study changes around specific places in the tropical Pacific (Elison Timm et al., 2015; Lauer et al., 2013; Xue et al., 2020; Zhang et al., 2016). Those methods offer at least an interim solution for assessing the likelihood of future climate changes on finer spatial scales than we considered in this study.

There are several future research opportunities besides addressing the questions and general limitations discussed above. In this study, we considered future changes to SST, rainfall, and SSH individually, although these variables are sometimes concurrently affected by many of the same climate variability processes (e.g., ENSO-associated extremes in the ocean and atmosphere; Holbrook et al., 2020) and long-term trends (e.g., a warming and rising ocean; see Table 3 for the regional sea level rise projections from Sweet et al. (2022)). Co-occurring or compounding weather and climate changes (Zscheischler et al., 2020) could amplify impacts in the tropical Pacific Islands. An example hazard of combined extremes is created when high sea levels occur with rainfall anomalies, which could stress coastal environments in a variety of ways, such as enhancing saltwater inundation (during droughts) or flooding (after heavy rainfall). Assessing the joint occurrences of climate anomalies in the CMIP6 projections are necessary to better describe the likelihood of changing hazards associated with combined extreme events (Raymond et al., 2020).

The availability of state-of-the-art climate change experiments from CMIP6 and our assessment of their GMST, SST, rainfall, and SSH output comes at a time when many Pacific Island communities are planning how they will adapt to continued greenhouse warming (Mcleod et al., 2019). In efforts to achieve the Sustainable Development Goals established by the United Nations, policymakers and other stakeholders are actively seeking to acquire the best available climate science to inform their decisions. Our assessment provides information about the large-scale climate changes in the tropical Pacific relative to the recent historical climatology that are projected to occur for 3°C of global warming since preindustrial levels. This amount of warming is almost certain to occur during the second half of the 21st century if the increase in greenhouse gas radiative forcing follows the SSP5-8.5 scenario. Lesser warming, for instance only a 1.5°C increase, could occur as soon as the end of this decade under

that scenario, or as late as the 2050s, according to a few of the models in the SSP2-4.5 experiment. In spite of great uncertainty about when particular warming amounts will be realized, we hope that our study provides useful information about climate changes that are likely to occur sometime during the 21st century.

Considering the vast geographical scope of the tropical Pacific, and the wide variety of climate changes projected by CMIP6 across the region, additional products are necessary for effectively communicating these results. The Pacific Islands Regional Climate Assessment (PIRCA) process, Pacific Climate Change Monitor (PCCM) reporting, and the next iteration of the U.S. National Climate Assessment (i.e., NCA5) are three such means for reporting on the best available climate science information at island-regional scales. New technology, such as the ability to efficiently describe the CMIP6 projections for any particular place, could enhance communication about likely climate changes, especially to traditionally underserved communities by this type of information.

Data Availability Statement

CMIP6 data provided by the Earth System Grid Federation (ESGF) can be accessed by the open-source link: https://esgf-node.llnl.gov/search/cmip6/. Users should select the models (source ID) and variables as indicated in Table 1, the frequency as monthly (mon), the variant label as r1i1p1f1 or the lowest available "r" number, and the experiment ID as either historical, ssp245, or ssp585. Data can be downloaded as NetCDF files that appear in the search outputs. Sea level rise projections are available in numerical form from the Interagency Sea Level Rise Scenario Tool (https://sealevel.nasa.gov/task-force-scenario-tool). The observational data used in this study are available from the following sources: GMST (https://www.metoffice.gov.uk/hadobs/hadcrut5/data/current/download.html), SST (https://psl.noaa.gov/data/gridded/data.noaa.ersst.v5.html), rainfall (https://psl.noaa.gov/data/gridded/data.gpcp.html), and SSH (https://resources.marine.copernicus.eu/product-detail/SEALEVEL_GLO_PHY_L4_MY_008_047/INFORMATION).

Acknowledgments
This study was supported by the NOAA Climate Program Office's Modeling, Analysis, Predictions, and Projections (MAPP) program through grant NA19OAR4310292. The authors acknowledge the helpful collaborations facilitated by the MAPP-organized CMIP6 Task Force, as well as insightful discussions with John Marra, Philip Thompson, Malte Stuecker, and Christina Karamperidou. The authors also acknowledge the World Climate Research Programme's Working Group on Coupled Modeling, which is responsible for CMIP, and the authors thank the climate modeling groups for producing and making available their model output. Comments from an associate editor and two anonymous reviewers greatly improved this study.

References

Adler, R. F., Sapiano, M. R., Huffman, G. J., Wang, J.-J., Gu, G., Bolvin, D., et al. (2018). The Global Precipitation Climatology Project (GPCP) monthly analysis (new version 2.3) and a review of 2017 global precipitation. *Atmosphere*, *9*(4), 138. https://doi.org/10.3390/atmos9040138

Alexander, M. A., Scott, J. D., Friedland, K. D., Mills, K. E., Nye, J. A., Pershing, A. J., & Thomas, A. C. (2018). Projected sea surface temperatures over the 21st century: Changes in the mean, variability and extremes for large marine ecosystem regions of Northern Oceans. *Elementa: Science of the Anthropocene*, *6*, 9. https://doi.org/10.1525/elementa.191

Allen, M., Dube, O., Solecki, W., Aragón-Durand, F., Cramer, W., Humphreys, S., et al. (2018). Global warming of 1.5°C. An IPCC Special Report on the impacts of global warming of 1.5°C above pre-industrial levels and related global greenhouse gas emission pathways, in the context of strengthening the global response to the threat of climate change, sustainable development, and efforts to eradicate poverty. In V. Masson-Delmotte, P. Zhai, H.-O. Pörtner, D. Roberts, J. Skea, P. R. Shukla, et al. (Eds.), *Sustainable development, and efforts to eradicate poverty*. Retrieved from https://www.ipcc.ch/

Annamalai, H., Hafner, J., Kumar, A., & Wang, H. (2014). A framework for dynamical seasonal prediction of precipitation over the Pacific islands. *Journal of Climate*, *27*(9), 3272–3297. https://doi.org/10.1175/JCLI-D-13-00379.1

Annamalai, H., Hafner, J., Sooraj, K., & Pillai, P. (2013). Global warming shifts the monsoon circulation, drying South Asia. *Journal of Climate*, *26*(9), 2701–2718. https://doi.org/10.1175/JCLI-D-12-00208.1

Beobide-Arsuaga, G., Bayr, T., Reintges, A., & Latif, M. (2021). Uncertainty of ENSO-amplitude projections in CMIP5 and CMIP6 models. *Climate Dynamics*, *56*(11–12), 3875–3888. https://doi.org/10.1007/s00382-021-05673-4

Berner, J., Christensen, H. M., & Sardeshmukh, P. D. (2020). Does ENSO regularity increase in a warming climate? *Journal of Climate*, *33*(4), 1247–1259. https://doi.org/10.1175/JCLI-D-19-0545.1

Bindoff, N. L., Stott, P. A., AchutaRao, K. M., Allen, M. R., Gillett, N., Gutzler, D., et al. (2013). Chapter 10 – Detection and attribution of climate change: From global to regional. In T. F. Stocker, D. Qin, G.-K. Plattner, M. Tignor, S. K. Allen, J. Boschung, et al. (Eds.), *Climate change 2013: The physical science basis. IPCC working group I contribution to AR5* (pp. 867–952). Cambridge University Press. Retrieved from https://www.ipcc.ch/

Bograd, S. J., Kang, S., Di Lorenzo, E., Horii, T., Katugin, O. N., King, J. R., et al. (2019). Developing a social–ecological–environmental system framework to address climate change impacts in the North Pacific. *Frontiers in Marine Science*, *6*, 333. https://doi.org/10.3389/fmars.2019.00333

Broccoli, A. J., Dahl, K. A., & Stouffer, R. J. (2006). Response of the ITCZ to Northern Hemisphere cooling. *Journal of Geophysical Research*, *33*(1). https://doi.org/10.1029/2005GL024546

Brown, J. R., Brierley, C. M., An, S.-I., Guarino, M.-V., Stevenson, S., Williams, C. J. R., et al. (2020). Comparison of past and future simulations of ENSO in CMIP5/PMIP3 and CMIP6/PMIP4 models. *Climate of the Past*, *16*(5), 1777–1805. https://doi.org/10.5194/cp-16-1777-2020

Brown, J. R., Lengaigne, M., Lintner, B. R., Widlansky, M. J., vander Wiel, K., Dutheil, C., et al. (2020). South Pacific Convergence Zone dynamics, variability and impacts in a changing climate. *Nature Reviews Earth & Environment*, *1*, 530–543. https://doi.org/10.1038/s43017-020-0078-2

Cai, W., Ng, B., Wang, G., Santoso, A., Wu, L., & Yang, K. (2022). Increased ENSO sea surface temperature variability under four IPCC emission scenarios. *Nature Climate Change*, *12*, 228–231. https://doi.org/10.1038/s41558-022-01282-z

Cai, W., Santoso, A., Collins, M., Dewitte, B., Karamperidou, C., Kug, J.-S., et al. (2021). Changing El Niño–Southern Oscillation in a warming climate. *Nature Reviews Earth & Environment*, *2*(9), 628–644. https://doi.org/10.1038/s43017-021-00199-z

Cai, W., Santoso, A., Wang, G., Yeh, S.-W., An, S.-I., Cobb, K. M., et al. (2015). ENSO and greenhouse warming. *Nature Climate Change*, *5*(9), 849–859. https://doi.org/10.1038/nclimate2743

Chadwick, R., Boutle, I., & Martin, G. (2013). Spatial patterns of precipitation change in CMIP5: Why the rich do not get richer in the tropics. *Journal of Climate*, *26*(11), 3803–3822. https://doi.org/10.1175/jcli-d-12-00543.1

Chou, C., Chiang, J. C. H., Lan, C.-W., Chung, C.-H., Liao, Y.-C., & Lee, C.-J. (2013). Increase in the range between wet and dry season precipitation. *Nature Geoscience*, *6*(4), 263–267. https://doi.org/10.1038/ngeo1744

Christensen, J. H., Kanikicharla, K. K., Aldrian, E., An, S. I., Cavalcanti, I. F. A., de Castro, M., et al. (2013). Climate phenomena and their relevance for future regional climate change. In T. F. Stocker, D. Qin, G.-K. Plattner, M. Tignor, S. K. Allen, J. Boschung, et al. (Eds.), *Climate change 2013: The physical science basis: Working group I contribution to the fifth assessment report of the intergovernmental panel on climate change* (pp. 1217–1308). Cambridge University Press. Retrieved from https://www.ipcc.ch/

Collins, M., An, S.-I., Cai, W., Ganachaud, A., Guilyardi, E., Jin, F.-F., et al. (2010). The impact of global warming on the tropical Pacific Ocean and El Niño. *Nature Geoscience*, *3*(6), 391–397. https://doi.org/10.1038/ngeo868

Curnock, M. I., Marshall, N. A., Thiault, L., Heron, S. F., Hoey, J., Williams, G., et al. (2019). Shifts in tourists' sentiments and climate risk perceptions following mass coral bleaching of the Great Barrier Reef. *Nature Climate Change*, *9*(7), 535–541. https://doi.org/10.1038/s41558-019-0504-y

Deo, R. C. (2011). On meteorological droughts in tropical Pacific islands: Time-series analysis of observed rainfall using Fiji as a case study. *Meteorological Applications*, *18*(2), 171–180. https://doi.org/10.1002/met.216

Doblas-Reyes, F., Sorensson, A., Almazroui, M., Dosio, A., Gutowski, W., Haarsma, R., et al. (2021). Linking global to regional climate change. In V. Masson-Delmotte, P. Zhai, A. Pirani, S. L. Connors, C. Péan, S. Berger, et al. (Eds.), *Climate change 2021: The physical science basis. Contribution of working group I to the sixth assessment report of the intergovernmental panel on climate change*. Cambridge University Press. Retrieved from https://www.ipcc.ch/

Dong, Y., Armour, K. C., Zelinka, M. D., Proistosescu, C., Battisti, D. S., Zhou, C., & Andrews, T. (2020). Intermodel spread in the pattern effect and its contribution to climate sensitivity in CMIP5 and CMIP6 models. *Journal of Climate*, *33*(18), 7755–7775. https://doi.org/10.1175/jcli-d-19-1011.1

Dutra, L. X. C., Haywood, M. D. E., Singh, S., Ferreira, M., Johnson, J. E., Veitayaki, J., et al. (2021). Synergies between local and climate-driven impacts on coral reefs in the tropical Pacific: A review of issues and adaptation opportunities. *Marine Pollution Bulletin*, *164*, 111922. https://doi.org/10.1016/j.marpolbul.2020.111922

Dwyer, J. G., Biasutti, M., & Sobel, A. H. (2012). Projected changes in the seasonal cycle of surface temperature. *Journal of Climate*, *25*(18), 6359–6374. https://doi.org/10.1175/JCLI-D-11-00741.1

Elison Timm, O., Giambelluca, T. W., & Diaz, H. F. (2015). Statistical downscaling of rainfall changes in Hawai'i based on the CMIP5 global model projections. *Journal of Geophysical Research: Atmospheres*, *120*(1), 92–112. https://doi.org/10.1002/2014jd022059

Eyring, V., Bony, S., Meehl, G. A., Senior, C. A., Stevens, B., Stouffer, R. J., & Taylor, K. E. (2016). Overview of the coupled model intercomparison project phase 6 (CMIP6) experimental design and organization. *Geoscientific Model Development*, *9*(5), 1937–1958. https://doi.org/10.5194/gmd-9-1937-2016

Fasullo, J. T., & Nerem, R. S. (2018). Altimeter-era emergence of the patterns of forced sea-level rise in climate models and implications for the future. *Proceedings of the National Academy of Sciences of the United States of America*, *115*(51), 12944–12949. https://doi.org/10.1073/pnas.1813233115

Fox-Kemper, B., Hewitt, H., Xiao, C., Aðalgeirsdóttir, G., Drijfhout, S., Edwards, T., et al. (2021). Ocean, cryosphere and sea level change. In V. Masson-Delmotte, P. Zhai, A. Pirani, S. L. Connors, C. Péan, N. C. S. Berger, et al. (Eds.), *Climate change 2021: The physical science basis. Contribution of working group I to the sixth assessment report of the intergovernmental panel on climate change*. Cambridge University Press. Retrieved from https://www.ipcc.ch/working-group/wg1/

Fredriksen, H. B., Berner, J., Subramanian, A. C., & Capotondi, A. (2020). How does El Niño–Southern Oscillation change under global warming—A first look at CMIP6. *Geophysical Research Letters*, *47*(22). https://doi.org/10.1029/2020gl090640

Giambelluca, T. W., Chen, Q., Frazier, A. G., Price, J. P., Chen, Y.-L., Chu, P.-S., et al. (2013). Online rainfall atlas of Hawai'i. *Bulletin of the American Meteorological Society*, *94*(3), 313–316. https://doi.org/10.1175/bams-d-11-00228.1

Giambelluca, T. W., Martin, R. E., Asner, G. P., Huang, M., Mudd, R. G., Nullet, M. A., et al. (2009). Evapotranspiration and energy balance of native wet montane cloud forest in Hawai 'i. *Agricultural and Forest Meteorology*, *149*(2), 230–243. https://doi.org/10.1016/j.agrformet.2008.08.004

Grose, M. R., Brown, J. N., Narsey, S., Brown, J. R., Murphy, B. F., Langlais, C., et al. (2014). Assessment of the CMIP5 global climate model simulations of the Western tropical Pacific climate system and comparison to CMIP3. *International Journal of Climatology*, *34*(12), 3382–3399. https://doi.org/10.1002/joc.3916

Guilyardi, E., Bellenger, H., Collins, M., Ferrett, S., Cai, W., & Wittenberg, A. (2012). A first look at ENSO in CMIP5. *CLIVAR Exchange*, *17*(58), 29–32.

Han, S. C., Sauber, J., Pollitz, F., & Ray, R. (2019). Sea level rise in the Samoan Islands escalated by viscoelastic relaxation after the 2009 Samoa-Tonga earthquake. *Journal of Geophysical Research: Solid Earth*, *124*(4), 4142–4156. https://doi.org/10.1029/2018jb017110

Hay, C. C., Morrow, E., Kopp, R. E., & Mitrovica, J. X. (2015). Probabilistic reanalysis of twentieth-century sea-level rise. *Nature*, *517*(7535), 481–484. https://doi.org/10.1038/nature14093

He, C., & Li, T. (2019). Does global warming amplify interannual climate variability? *Climate Dynamite*, *52*(5–6), 2667–2684. https://doi.org/10.1007/s00382-018-4286-0

Held, I. M., & Soden, B. J. (2006). Robust responses of the hydrological cycle to global warming. *Journal of Climate*, *19*(21), 5686–5699. https://doi.org/10.1175/JCLI3990.1

Herger, N., Sanderson, B. M., & Knutti, R. (2015). Improved pattern scaling approaches for the use in climate impact studies. *Geophysical Research Letters*, *42*(9), 3486–3494. https://doi.org/10.1002/2015GL063569

Hoeke, R. K., McInnes, K. L., Kruger, J. C., McNaught, R. J., Hunter, J. R., & Smithers, S. G. (2013). Widespread inundation of Pacific islands triggered by distant-source wind-waves. *Global and Planetary Change*, *108*, 128–138. https://doi.org/10.1016/j.gloplacha.2013.06.006

Holbrook, N. J., Claar, D. C., Hobday, A. J., McInnes, K. L., Oliver, E. C., Gupta, A. S., et al. (2020). Chapter 18 – ENSO-driven ocean extremes and their ecosystem impacts. In *El Niño Southern Oscillation in a changing climate* (pp. 409–428). John Wiley & Sons, Inc. https://doi.org/10.1002/9781119548164.ch18

Huang, P., Xie, S.-P., Hu, K., Huang, G., & Huang, R. (2013). Patterns of the seasonal response of tropical rainfall to global warming. *Nature Geoscience*, *6*(5), 357–361. https://doi.org/10.1038/ngeo1792

Jin, F.-F., Neelin, J. D., & Ghil, M. (1994). El Niño on the devil's staircase: Annual subharmonic steps to chaos. *Science*, *264*(5155), 70–72. https://doi.org/10.1126/science.264.5155.70

Johnson, N. C., & Xie, S.-P. (2010). Changes in the sea surface temperature threshold for tropical convection. *Nature Geoscience*, *3*(12), 842–845. https://doi.org/10.1038/ngeo1008

Karamperidou, C., Stuecker, M. F., Timmermann, A., Yun, K. S., Lee, S. S., Jin, F. F., et al. (2020). Chapter 21 – ENSO in a changing climate: Challenges, paleo-perspectives, and outlook. In *El Niño Southern Oscillation in a changing climate* (pp. 471–484). John Wiley & Sons, Inc. https://doi.org/10.1002/9781119548164.ch21

Keener, V., Helweg, D., Asam, S., Balwani, S., Burkett, M., Fletcher, C., et al. (2018). Hawai 'i and US-affiliated Pacific Islands. *Impacts, risks and adaptation in the United States: Fourth National Climate Assessment* (Vol. II, pp. 1242–1308). US Global Change Research Program.

Lauer, A., Zhang, C., Elison-Timm, O., Wang, Y., & Hamilton, K. (2013). Downscaling of climate change in the Hawaii region using CMIP5 results: On the choice of the forcing fields. *Journal of Climate*, *26*(24), 10006–10030. https://doi.org/10.1175/jcli-d-13-00126.1

Lee, J., Marotzke, J., Bala, G., Cao, L., Corti, S., Dunne, J., et al. (2021). Future global climate: Scenario-based projections and near-term information. In V. Masson-Delmotte, P. Zhai, A. Pirani, S. L. Connors, C. Péan, S. Berger, et al. (Eds.), *Climate change 2021: The physical science basis. Contribution of working group I to the sixth assessment report of the intergovernmental panel on climate change* (p. 195). Cambridge University Press. Retrieved from https://www.ipcc.ch/report/ar6/wg1/

Lehodey, P., Bertrand, A., Hobday, A. J., Kiyofuji, H., McClatchie, S., Menkès, C. E., et al. (2020). Chapter 19 – ENSO impact on marine fisheries and ecosystems. In *El Niño Southern Oscillation in a changing climate* (1st ed., pp. 429–451). John Wiley & Sons, Inc. https://doi.org/10.1002/9781119548164.ch19

Li, G., Xie, S.-P., Du, Y., & Luo, Y. (2016). Effects of excessive equatorial cold tongue bias on the projections of tropical Pacific climate change. Part I: The warming pattern in CMIP5 multi-model ensemble. *Climate Dynamite*, *47*(12), 3817–3831. https://doi.org/10.1007/s00382-016-3043-5

Li, J. L., Xu, K. M., Jiang, J., Lee, W. L., Wang, L. C., Yu, J. Y., et al. (2020). An overview of CMIP5 and CMIP6 simulated cloud ice, radiation fields, surface wind stress, sea surface temperatures, and precipitation over tropical and subtropical oceans. *Journal of Geophysical Research: Atmospheres*, *125*(15), e2020JD032848. https://doi.org/10.1029/2020JD032848

Long, X., Widlansky, M. J., Schloesser, F., Thompson, P. R., Annamalai, H., Merrifield, M. A., & Yoon, H. (2020). Higher sea levels at Hawaii caused by strong El Niño and weak trade winds. *Journal of Climate*, *33*(8), 3037–3059. https://doi.org/10.1175/jcli-d-19-0221.1

Longman, R. J., Elison Timm, O., Giambelluca, T. W., & Kaiser, L. (2021). A 20-year analysis of disturbance-driven rainfall on O'ahu, Hawai'i. *Monthly Weather Review*, *149*(6), 1767–1783. https://doi.org/10.1175/mwr-d-20-0287.1

Lorrey, A. M., & Fauchereau, N. C. (2018). Southwest Pacific atmospheric weather regimes: Linkages to ENSO and extra-tropical teleconnections. *International Journal of Climatology*, *38*(4), 1893–1909. https://doi.org/10.1002/joc.5304

Marvel, K., Biasutti, M., Bonfils, C., Taylor, K. E., Kushnir, Y., & Cook, B. I. (2017). Observed and projected changes to the precipitation annual cycle. *Journal of Climate*, *30*(13), 4983–4995. https://doi.org/10.1175/jcli-d-16-0572.1

Mcleod, E., Bruton-Adams, M., Förster, J., Franco, C., Gaines, G., Gorong, B., et al. (2019). Lessons from the Pacific Islands—Adapting to climate change by supporting social and ecological resilience. *Frontiers in Marine Science*, *6*, 289. https://doi.org/10.3389/fmars.2019.00289

McPhaden, M. J., Santoso, A., & Cai, W. (2020). *El Niño Southern Oscillation in a changing climate* (1st ed., Vol. 253). John Wiley & Sons.

Meehl, G. A., Senior, C. A., Eyring, V., Flato, G., Lamarque, J.-F., Stouffer, R. J., et al. (2020). Context for interpreting equilibrium climate sensitivity and transient climate response from the CMIP6 Earth system models. *Science Advances*, *6*(26). https://doi.org/10.1126/sciadv.aba1981

Morice, C. P., Kennedy, J. J., Rayner, N. A., Winn, J. P., Hogan, E., Killick, R. E., et al. (2021). An updated assessment of near-surface temperature change from 1850: The HadCRUT5 data set. *Journal of Geophysical Research: Atmospheres*, *126*(3). https://doi.org/10.1029/2019jd032361

O'Neill, B. C., Kriegler, E., Riahi, K., Ebi, K. L., Hallegatte, S., Carter, T. R., et al. (2014). A new scenario framework for climate change research: The concept of shared socioeconomic pathways. *Climate Change*, *122*(3), 387–400. https://doi.org/10.1007/s10584-013-0905-2

Oueslati, B., & Bellon, G. (2015). The double ITCZ bias in CMIP5 models: Interaction between SST, large-scale circulation and precipitation. *Climate Dynamite*, *44*(3–4), 585–607. https://doi.org/10.1007/s00382-015-2468-6

Pendergrass, A. G., Knutti, R., Lehner, F., Deser, C., & Sanderson, B. M. (2017). Precipitation variability increases in a warmer climate. *Scientific Reports*, *7*(1). https://doi.org/10.1038/s41598-017-17966-y

Power, S. B., Delage, F., Colman, R., & Moise, A. (2012). Consensus on twenty-first-century rainfall projections in climate models more widespread than previously thought. *Journal of Climate*, *25*(11), 3792–3809. https://doi.org/10.1175/jcli-d-11-00354.1

Power, S. B., Lengaigne, M., Capotondi, A., Khodri, M., Vialard, J., Jebri, B., et al. (2021). Decadal climate variability in the tropical Pacific: Characteristics, causes, predictability, and prospects. *Science*, *374*(6563), eaay9165. https://doi.org/10.1126/science.aay9165

Pujol, M.-I., Faugère, Y., Taburet, G., Dupuy, S., Pelloquin, C., Ablain, M., & Picot, N. (2016). DUACS DT2014: The new multi-mission altimeter data set reprocessed over 20 years. *Ocean Science*, *12*(5), 1067–1090. https://doi.org/10.5194/os-12-1067-2016

Raymond, C., Horton, R. M., Zscheischler, J., Martius, O., Aghakouchak, A., Balch, J., et al. (2020). Understanding and managing connected extreme events. *Nature Climate Change*, *10*(7), 611–621. https://doi.org/10.1038/s41558-020-0790-4

Reynolds, R. W., Rayner, N. A., Smith, T. M., Stokes, D. C., & Wang, W. (2002). An improved in situ and satellite SST analysis for climate. *Journal of Climate*, *15*(13), 1609–1625. https://doi.org/10.1175/1520-0442(2002)015<1609:aiisas>2.0.co;2

Riahi, K., vanVuuren, D. P., Kriegler, E., Edmonds, J., O'Neill, B. C., Fujimori, S., et al. (2017). The shared socioeconomic pathways and their energy, land use, and greenhouse gas emissions implications: An overview. *Global and Planetary Change*, *42*, 153–168. https://doi.org/10.1016/j.gloenvcha.2016.05.009

Roca, R., Alexander, L. V., Potter, G., Bador, M., Jucá, R., Contractor, S., et al. (2019). FROGS: A daily $1° \times 1°$ gridded precipitation database of rain gauge, satellite and reanalysis products. *Earth System Science Data*, *11*(3), 1017–1035. https://doi.org/10.5194/essd-11-1017-2019

Rogelj, J., Popp, A., Calvin, K. V., Luderer, G., Emmerling, J., Gernaat, D., et al. (2018). Scenarios towards limiting global mean temperature increase below 1.5°C. *Nature Climate Change*, *8*(4), 325–332. https://doi.org/10.1038/s41558-018-0091-3

Samanta, D., Karnauskas, K. B., & Goodkin, N. F. (2019). Tropical Pacific SST and ITCZ biases in climate models: Double trouble for future rainfall projections? *Geophysical Research Letters*, *46*(4), 2242–2252. https://doi.org/10.1029/2018gl081363

Seager, R., Naik, N., & Vecchi, G. A. (2010). Thermodynamic and dynamic mechanisms for large-scale changes in the hydrological cycle in response to global warming. *Journal of Climate*, *23*(17), 4651–4668. https://doi.org/10.1175/2010jcli3655.1

Seth, A., Rauscher, S. A., Biasutti, M., Giannini, A., Camargo, S. J., & Rojas, M. (2013). CMIP5 projected changes in the annual cycle of precipitation in monsoon regions. *Journal of Climate*, *26*(19), 7328–7351. https://doi.org/10.1175/JCLI-D-12-00726.1

Stevenson, S. (2012). Significant changes to ENSO strength and impacts in the twenty-first century: Results from CMIP5. *Geophysical Research Letters*, *39*(17). https://doi.org/10.1029/2012GL052759

Sweet, W. V., Hamlington, B. D., Kopp, R. E., Weaver, C. P., Barnard, P. L., Bekaert, D., et al. (2022). *Global and regional sea level rise scenarios for the United States: Updated mean projections and extreme water level probabilities along U.S. coastlines*. National Oceanic and Atmospheric Administration, National Ocean Service. Retrieved from https://oceanservice.noaa.gov/hazards/sealevelrise/noaa-nos-techrpt01-global-regional-SLR-scenarios-US.pdf

Taschetto, A. S., Gupta, A. S., Jourdain, N. C., Santoso, A., Ummenhofer, C. C., & England, M. H. (2014). Cold tongue and warm pool ENSO events in CMIP5: Mean state and future projections. *Journal of Climate*, *27*(8), 2861–2885. https://doi.org/10.1175/jcli-d-13-00437.1

Taylor, K. E., Stouffer, R. J., & Meehl, G. A. (2012). An overview of CMIP5 and the experiment design. *Bulletin of the American Meteorological Society*, *93*(4), 485–498. https://doi.org/10.1175/bams-d-11-00094.1

Thomson, R. E., & Emery, W. J. (2014). *Data analysis methods in physical oceanography*. Newnes.

Timmermann, A., Jin, F. F., & Collins, M. (2004). Intensification of the annual cycle in the tropical Pacific due to greenhouse warming. *Geophysical Research Letters*, *31*(12). https://doi.org/10.1029/2004GL019442

Timmermann, A., McGregor, S., & Jin, F.-F. (2010). Wind effects on past and future regional sea level trends in the southern Indo-Pacific. *Journal of Climate*, *23*(16), 4429–4437. https://doi.org/10.1175/2010jcli3519.1

Tziperman, E., Stone, L., Cane, M. A., & Jarosh, H. (1994). El Niño chaos: Overlapping of resonances between the seasonal cycle and the Pacific ocean-atmosphere oscillator. *Science*, *264*(5155), 72–74. https://doi.org/10.1126/science.264.5155.72

Venegas, R., Oliver, T., Brainard, R. E., Santos, M., Geronimo, R., & Widlansky, M. (2019). Climate-induced vulnerability of fisheries in the Coral Triangle: Skipjack Tuna thermal spawning habitats. *Fisheries Oceanography*, *28*(2), 117–130. https://doi.org/10.1111/fog.12390

Wengel, C., Lee, S.-S., Stuecker, M. F., Timmermann, A., Chu, J.-E., & Schloesser, F. (2021). Future high-resolution El Niño/Southern Oscillation dynamics. *Nature Climate Change*, *11*(9), 758–765. https://doi.org/10.1038/s41558-021-01132-4

Widlansky, M. J., Long, X., & Schloesser, F. (2020). Increase in sea level variability with ocean warming associated with the nonlinear thermal expansion of seawater. *Communications Earth & Environment*, *1*(1). https://doi.org/10.1038/s43247-020-0008-8

Widlansky, M. J., Timmermann, A., & Cai, W. (2015). Future extreme sea level seesaws in the tropical Pacific. *Science Advances*, *1*(8). https://doi.org/10.1126/sciadv.1500560

Widlansky, M. J., Timmermann, A., McGregor, S., Stuecker, M. F., & Cai, W. (2014). An interhemispheric tropical sea level seesaw due to El Niño Taimasa. *Journal of Climate*, *27*(3), 1070–1081. https://doi.org/10.1175/jcli-d-13-00276.1

Widlansky, M. J., Timmermann, A., Stein, K., McGregor, S., Schneider, N., England, M. H., et al. (2013). Changes in South Pacific rainfall bands in a warming climate. *Nature Climate Change*, *3*(4), 417–423. https://doi.org/10.1038/nclimate1726

Widlansky, M. J., Webster, P. J., & Hoyos, C. D. (2011). On the location and orientation of the South Pacific convergence zone. *Climate Dynamite*, *36*(3–4), 561–578. https://doi.org/10.1007/s00382-010-0871-6

Xue, L., Wang, Y., Newman, A. J., Ikeda, K., Rasmussen, R. M., Giambelluca, T. W., et al. (2020). How will rainfall change over Hawai ʻi in the future? High-resolution regional climate simulation of the Hawaiian Islands. *Bulletin of Atmospheric Science and Technology*, *1*(3), 459–490. https://doi.org/10.1007/s42865-020-00022-5

Yeh, S.-W., Ham, Y.-G., & Lee, J.-Y. (2012). Changes in the tropical Pacific SST trend from CMIP3 to CMIP5 and its implication of ENSO. *Journal of Climate*, *25*(21), 7764–7771. https://doi.org/10.1175/jcli-d-12-00304.1

Ying, J., Collins, M., Cai, W., Timmermann, A., Huang, P., Chen, D., & Stein, K. (2022). Emergence of climate change in the tropical Pacific. *Nature Climate Change*. https://doi.org/10.1038/s41558-022-01301-z

Yun, K.-S., Lee, J.-Y., Timmermann, A., Stein, K., Stuecker, M. F., Fyfe, J. C., & Chung, E.-S. (2021). Increasing ENSO–rainfall variability due to changes in future tropical temperature–rainfall relationship. *Communications Earth & Environment*, *2*(1). https://doi.org/10.1038/s43247-021-00108-8

Zelinka, M. D., Myers, T. A., McCoy, D. T., Po-Chedley, S., Caldwell, P. M., Ceppi, P., et al. (2020). Causes of higher climate sensitivity in CMIP6 models. *Geophysical Research Letters*, *47*(1). https://doi.org/10.1029/2019gl085782

Zhang, C., Wang, Y., Hamilton, K., & Lauer, A. (2016). Dynamical downscaling of the climate for the Hawaiian Islands. Part I: Present day. *Journal of Climate*, *29*(8), 3027–3048. https://doi.org/10.1175/jcli-d-15-0432.1

Zhao, S., Jin, F. F., Long, X., & Cane, M. A. (2021). On the breakdown of ENSO's relationship with thermocline depth in the central-equatorial Pacific. *Geophysical Research Letters*, *48*(9). https://doi.org/10.1029/2020GL092335

Zscheischler, J., Martius, O., Westra, S., Bevacqua, E., Raymond, C., Horton, R. M., et al. (2020). A typology of compound weather and climate events. *Nature Reviews Earth & Environment*, *1*(7), 333–347. https://doi.org/10.1038/s43017-020-0060-z